Stem Cell Reports
Article

OPEN ACCESS

Leptin Receptor Signaling Regulates Protein Synthesis Pathways and Neuronal Differentiation in Pluripotent Stem Cells

Manoj K. Gupta,[1,2] Heidrun Vethe,[1,3] Samir Softic,[4,5] Tata Nageswara Rao,[1,10] Vilas Wagh,[6] Jun Shirakawa,[1,2] Harald Barsnes,[3,7] Marc Vaudel,[3,7] Tomozumi Takatani,[1,2] Sevim Kahraman,[1,2] Masaji Sakaguchi,[5] Rachael Martinez,[1] Jiang Hu,[1] Yngvild Bjørlykke,[3,8] Helge Raeder,[3,8] and Rohit N. Kulkarni[1,2,9,*]

[1]Section on Islet Cell and Regenerative Biology, Joslin Diabetes Center, Harvard Medical School, Boston, MA 02215, USA
[2]Department of Medicine, Brigham and Women's Hospital, Harvard Medical School, Boston, MA 02215, USA
[3]KG Jebsen Center for Diabetes Research, Department of Clinical Medicine, University of Bergen, Bergen 5009, Norway
[4]Department of Gastroenterology, Boston Children's Hospital, Harvard Medical School, Boston, MA 02215, USA
[5]Section of Integrative Physiology and Metabolism, Joslin Diabetes Center, Harvard Medical School, Boston, MA 02215, USA
[6]Center for Human Genetic Research, Massachusetts General Hospital, Boston, MA 02114, USA
[7]Proteomics Unit, Department of Biomedicine, University of Bergen, Norway
[8]Department of Pediatrics, Haukeland University Hospital, N-5021 Bergen, Norway
[9]Harvard Stem Cell Institute, Harvard Medical School, Boston, MA 02215, USA
[10]University Clinic of Hematology, Department of Biomedical Research, Inselspital Bern and University of Bern, Bern, Switzerland
*Correspondence: rohit.kulkarni@joslin.harvard.edu
https://doi.org/10.1016/j.stemcr.2020.10.001

SUMMARY

The role of leptin receptor (OB-R) signaling in linking pluripotency with growth and development and the consequences of dysfunctional leptin signaling on progression of metabolic disease is poorly understood. Using a global unbiased proteomics approach we report that embryonic fibroblasts (MEFs) carrying the db/db mutation exhibit metabolic abnormalities, while their reprogrammed induced pluripotent stem cells (iPSCs) show altered expression of proteins involved in embryonic development. An upregulation in expression of eukaryotic translation initiation factor 4e (*Eif4e*) and *Stat3* binding to the *Eif4e* promoter was supported by enhanced protein synthesis in mutant iPSCs. Directed differentiation of db/db iPSCs toward the neuronal lineage showed defects. Gene editing to correct the point mutation in db/db iPSCs using CRISPR-Cas9, restored expression of neuronal markers and protein synthesis while reversing the metabolic defects. These data imply a direct role for OB-R in regulating metabolism in embryonic fibroblasts and key developmental pathways in iPSCs.

INTRODUCTION

Mutations in different exons in the leptin receptor (OB-R) gene have been reported to cause obesity, pituitary dysfunction, and metabolic abnormalities in humans (Clement et al., 1998; Saeed et al., 2014). The db/db mouse, which harbors a mutation in the OB-R gene (G to T transition in the intron region between exon 18 and exon 19), manifests features that are strikingly similar to those seen in humans carrying the mutant receptor, such as obesity, type 2 diabetes, and tumorigenesis (Chen et al., 1996; Kobayashi et al., 2000; Wang et al., 2014). Thus, the db/db mouse continues to be widely used as a suitable model to explore the role of OB-R in the development and progression of obesity, diabetes, and its related complications.

While a majority of circulating leptin originates from adipose tissue, other tissues also contribute, such as the placenta, ovaries, testes, skeletal muscle, cartilage, bone cells, and stomach (Margetic et al., 2002). Following secretion leptin acts mainly via the OB-R, of which several isoforms exist, differing mainly in the length of the cytoplasmic domain (Chen et al., 1996). In addition to expression in adult tissues, such as the heart, pancreatic beta-cells, and immune cells the OB-R has been detected in fetal and developmental tissues, including placenta, endometrium, and pluripotent stem cells (El-Hefnawy et al., 2000; Hoggard et al., 2001). Furthermore, leptin, secreted by fibroblasts, has been reported to support proliferation of human pluripotent stem cells (Anisimov et al., 2011) and a previous study demonstrated binding of pluripotency factors, *Oct4* and *Sox2*, on the promoter region of *OB-R* (Feldman et al., 2012). Recently, leptin signaling has been suggested to regulate the parasympathetic nervous system during early embryonic development (Croizier et al., 2016). Thus, while studies point to a role for leptin receptors during early development the direct functional role of OB-R in modulating pluripotency and its consequences on development is unknown.

In this study, we used mouse embryonic fibroblasts (MEFs) and iPSCs derived from db/db mice as complementary model systems to explore OB-R signaling in the regulation of pluripotency and metabolic/mitochondrial function during embryonic development. Strikingly, db/db MEFs exhibited an upregulated ERK pathway and metabolic dysfunction, while db/db iPSCs showed reduced pluripotency and differential regulation of protein synthesis pathways. The latter defects in iPSCs were reversed upon correction of the db/db point mutation by genome editing using the clustered regularly interspaced short palindromic repeats (CRISPR-Cas9) approach. These findings were supported by RNA sequencing (RNA-seq) analyses on iPSCs. Furthermore, we report a role for OB-R signaling during neuronal development. Together these data indicate the significance of the OB-R in regulating genes/proteins relevant for pluripotency, protein synthesis pathways, and neuronal development with potential implications for cancer and metabolic diseases.

RESULTS

Functional Characterization and Global Proteomics Reveal Metabolic Abnormalities in Embryonic db/db MEFs

Global differential protein expression between Ctrl and db/db MEFs, investigated by mass spectrometry-based proteomics, revealed 38 strongly and 92 moderately regulated proteins that were significantly different between groups (detailed in the Experimental Procedures). The most differentially regulated proteins between Ctrl and db/db MEFs were those related to mitochondrial function and oxidative phosphorylation. The differentially regulated proteins and pathways are listed in Table S1 (Figures 1A, S1A, and S1B).

The most differentially regulated pathways included mitochondrial dysfunction, oxidative phosphorylation, and integrin signaling, while the moderately regulated pathways were insulin growth factor 1 signaling, cell cycle, BMP signaling, DNA methylation, molecular mechanisms of cancer, adipogenesis, leptin signaling in obesity, and protein ubiquitination. The complete list of regulated pathways is presented in Table S2.

To validate the key pathways we began with morphological characterization and observed larger MEFs in the db/db group (Figure S1C). We observed an upregulation of phosphorylation of MEK1/2, ERK1/2, and RAPTOR in db/db MEFs (Figure 1B), and the abundance of CDKN2a was upregulated in these MEFs (Figure S1D). Together, these data point to differential regulation of the MEK/ERK/RAPTOR pathway and mitochondrial dysfunction in db/db MEFs during embryonic development and suggest a link between OB-R and obesity and oncogenesis.

db/db iPSCs Show Altered Morphology and Pluripotency Characteristics

We confirmed the persistence of the leptin receptor mutation (G to T transition) in the db/db group by sequencing genomic DNA (Figures 1C and S2A). While no difference in colony morphology was evident between the two groups, a significantly larger cell size was detected in db/db iPSCs (Figures 1D and S2B). Interestingly, western blot analysis showed significant downregulation of Oct4 and Nanog protein levels in db/db iPSCs (Figures 1E–1G).

To explore their ability to spontaneously differentiate *in vivo* into the three germ layers we injected Ctrl or db/db iPSCs (1×10^6 cells/mouse) either subcutaneously or intramuscularly into severe combined immunodeficient (immunodeficient) and B6 (syngeneic) mice. As expected, we observed teratomas in both groups and the presence of β-III-tubulin (ectoderm in green), α-actinin (mesoderm in green), and HNF-3-β (endoderm in red) (Figures S2C and S2D) confirmed components of the three germ layers.

Global Proteomics Analyses of Ctrl and db/db iPSCs Reveals Differentially Regulated Pathways Associated with Pluripotency and Protein Synthesis

To interrogate changes in the global proteome we undertook systematic comparisons between MEFs and iPSCs separately in Ctrl and db/db groups as well as Ctrl iPSCs versus db/db iPSCs. We identified 665 strongly regulated proteins and 278 moderately regulated proteins that were significantly different between the two cell types (Ctrl MEFs versus Ctrl iPSCs) (Table S3). A comparison between db/db MEFs and db/db iPSCs, revealed 789 strongly regulated proteins and 271 moderately regulated proteins that reached statistical significance (Table S4). Comparing the proteome between Ctrl and db/db iPSCs, we identified 32 significantly and moderately regulated proteins (Table S5).

Next, to assess the specific effects of leptin signaling at the proteome level in pluripotent stem cells, we aimed to identify a protein signature consequent to deregulated OB-R signaling in induced pluripotent stem cells derived from db/db mice. The heatmap analyses revealed that mitochondrial proteins, protein synthesis, and pluripotent pathways were differentially regulated between Ctrl and db/db iPSCs (Figures 1H and S3A). As expected, iPSCs from Ctrl and db/db showed fewer differences in proteomic changes than the differentiated MEFs from the two respective groups. Specifically, up to 150 proteins were significantly differently expressed in the db/db MEF-specific proteome compared with 75 in the db/db iPSC-specific proteome, with five proteins being significantly differently expressed in both proteomes (Figure 1I).

Notably, many of the highly regulated proteins in the db/db MEF-specific proteome did not persist in the iPSC-specific proteome, suggesting a shutdown or suppression of db/db-specific proteins and pathways after the MEF cells were reprogrammed into pluripotent cells (Figures 1I and 1J).

Upregulated Eukaryotic Translation Initiation Factor 4E Protein Synthesis Pathway and Higher Metabolic Rates in Db/db iPSCs

Proteomic analyses revealed an upregulation of the eukaryotic translation initiation factor 4e (EIF4E) protein synthesis pathway among the canonical networks in the iPSCs of db/db mice. The complete list of differentially regulated

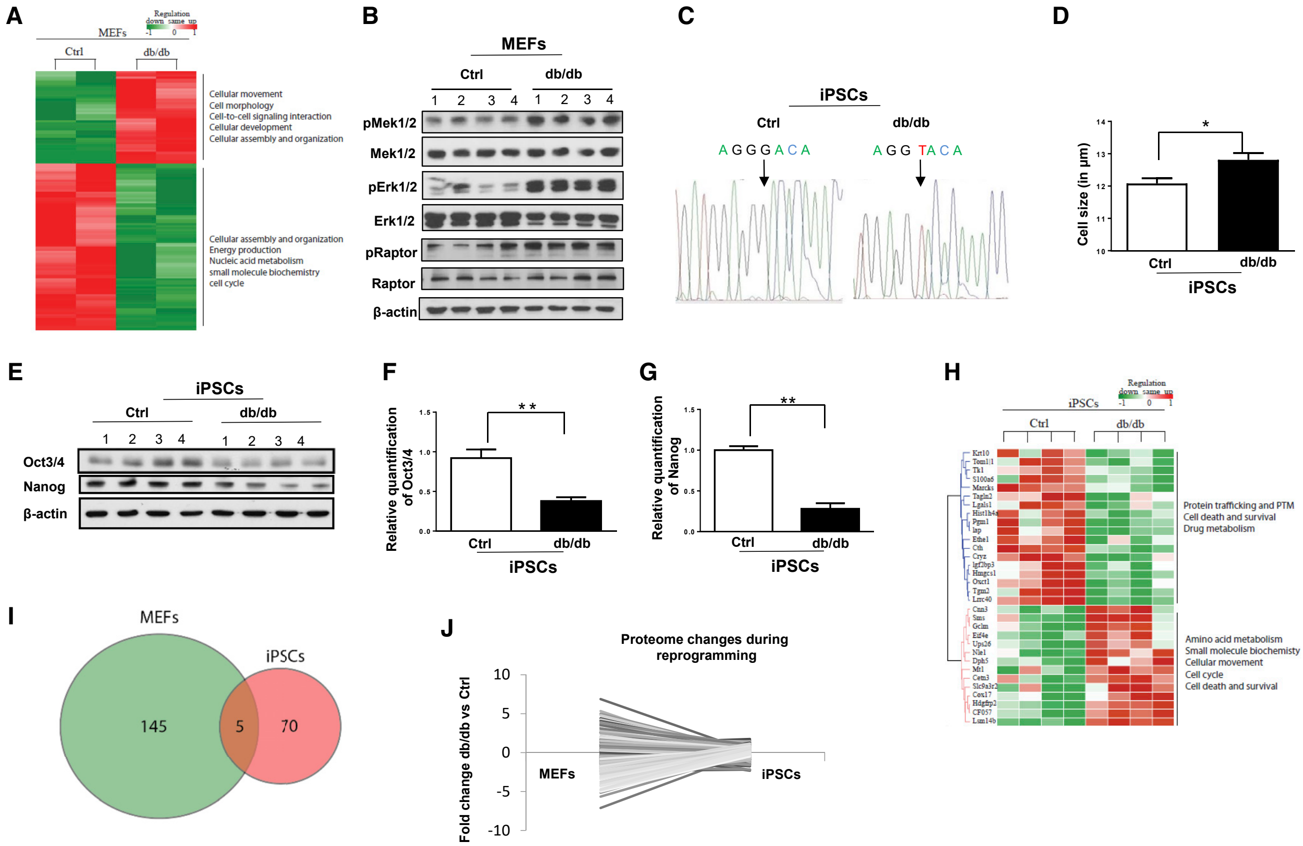

Figure 1. Altered Metabolic Regulation in db/db MEFs and Reduced Pluripotency and Upregulated Protein Synthesis Pathway in db/db iPSCs

(A–G) (A) Heatmap representation of differentially expressed proteins between Ctrl and db/db MEFs. A selection of gene ontology terms is given for each protein cluster. Red indicates upregulated while green indicates downregulated proteins in db/db MEFs. (B) Western blots analysis showing upregulated MEK1/2, ERK1/2, and RAPTOR pathways in db/db MEFs. β-Actin was used as a loading control. (C) Genomic DNA sequencing showing G to T transition of base in db/db iPSCs. (D) Cell diameter of Ctrl and db/db iPSCs using Cello meter. (E) Western blot analysis of OCT4 and NANOG in four different clones from Ctrl and db/db iPSCs; quantification of changes in OCT4 (F) and NANOG (G) using ImageJ software. β-Actin was used as a loading control.

(H–J) (H) Heatmap representation of pathway analysis of differentially expressed proteins between Ctrl and db/db iPSCs. A selection of GO terms is given for each protein cluster. Red indicates upregulated while green indicates downregulated proteins in db/db iPSCs. (I) Venn diagram showing the numbers of proteins that were significantly differently expressed ($p < 0.05$) in db/db MEF-specific proteome and the db/db iPSC-specific proteome. Five proteins were significantly changed between db/db and Ctrl, both before and after reprogramming. (J) Pairing of protein expression values from each of the significant proteins in the db/db MEF-specific proteome with the db/db iPSC-specific proteome.

pathways is available in Table S2 (Figures S3A and S3B; Tables S2 and S5).

We next considered previous reports that tissues manifesting the db/db mutation exhibit altered signal transducer and activator of transcription 3 (STAT3) signaling. Interestingly, while the effects of the db/db mutation have been observed in the hypothalamus (Ghilardi et al., 1996) leptin has been reported not to activate the Stat pathway in other adult tissues (Vaisse et al., 1996). The latter prompted us, for the first time, to examine STAT3 activation in iPSCs. In the unstimulated state, Ctrl iPSCs showed higher phosphorylation of STAT3, which robustly increased after stimulation with leukemia inhibitory factor (LIF) or leptin. The mutant db/db iPSCs showed a similar level of phosphorylation of STAT3 as compared with Ctrl iPSCs in the unstimulated state. Although db/db iPSCs also demonstrated phosphorylation of STAT3 after stimulation with LIF, the effect was significantly blunted after leptin stimulation indicating defective signaling (Figure S3C). Furthermore, OCT4 protein abundance was decreased in db/db iPSCs in the starved condition similar to that in the basal state.

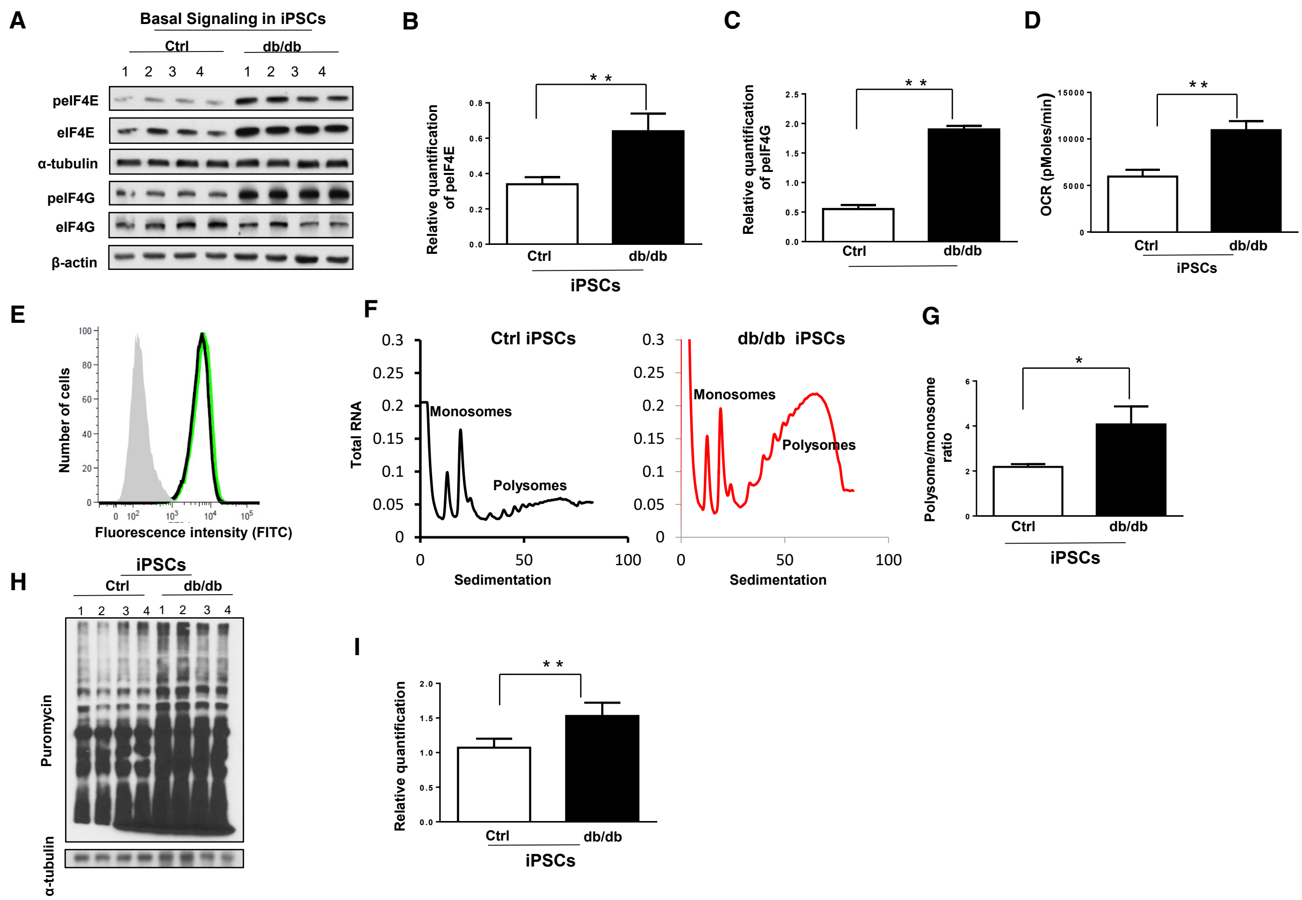

Figure 2. Upregulated Protein Synthesis in db/db iPSCs

(A–E) (A) Western blot analysis showing increase in phospho-EIF4E, phopho-EIF4G, and total EIF4E in db/db iPSCs. (B and C) quantification of the data in (A) phospho-EIF4E (B) and phospho-EIF4G (C). (D) metabolic profiling by Seahorse showing higher oxygen consumption rate (OCR) in db/db iPSCs as compared with Ctrl iPSCs. (E) Flow cytometry analysis showing relative higher mitochondrial mass (Mito-GFP) in db/db iPSCs.

(F–I) (F) Representative polysome profiling graphs showing polysome and monosome peaks in Ctrl (left panel, in black) and db/db iPSCs (right panel, in red). (G) Quantification of polysome and monosome ratios in both groups. (H) Anti-puromycin western blot analysis demonstrated higher protein synthesis in db/db iPSCs as compared with Ctrl iPSCs. α-Tubulin was used as a loading control. (I) Quantification of newly synthesized proteins in Ctrl and db/db iPSCs using α-tubulin as a loading control. n = 3 independent experiments; data are shown as mean ± SD by Student's t test (*p < 0.05, **p < 0.01).

EIF4E, as well as phosphorylated EIF4E, were significantly upregulated in the basal state, in agreement with mass spectrometry data on db/db iPSCs (Figures S3A and S3B). Phosphorylated EIF4G was also significantly upregulated in db/db iPSCs in the basal state as compared with Ctrl iPSCs (Figures 2A–2C). These results indicate that disrupted leptin receptor signaling leads to higher abundance of proteins that regulate protein synthesis in the pluripotent stage.

Next, metabolic profiling revealed higher basal oxygen consumption rate (OCR) in db/db iPSCs, indicating an increased metabolic rate/oxidative phosphorylation (OXPHOS) compared with Ctrl iPSCs (Figure 2D). Electron microscopy and flow cytometry analysis revealed relatively higher mitochondrial numbers in db/db iPSCs (Figures 2E and S4A). There was also a significant upregulation in the expression of *Pgc*-beta and *G6pd* genes in db/db iPSCs as compared with Ctrl iPSCs (Figures S4B and S4C). Together, these data suggest that the presence of the db/db mutation is associated with higher metabolic activity in the iPSCs.

Polysome Profiling Reveals Higher Protein Synthesis in db/db iPSCs: Role of Stat3 Binding to eIF4E Promoter

Since proteins related to protein synthesis were upregulated in db/db iPSCs, we undertook polysome profiling

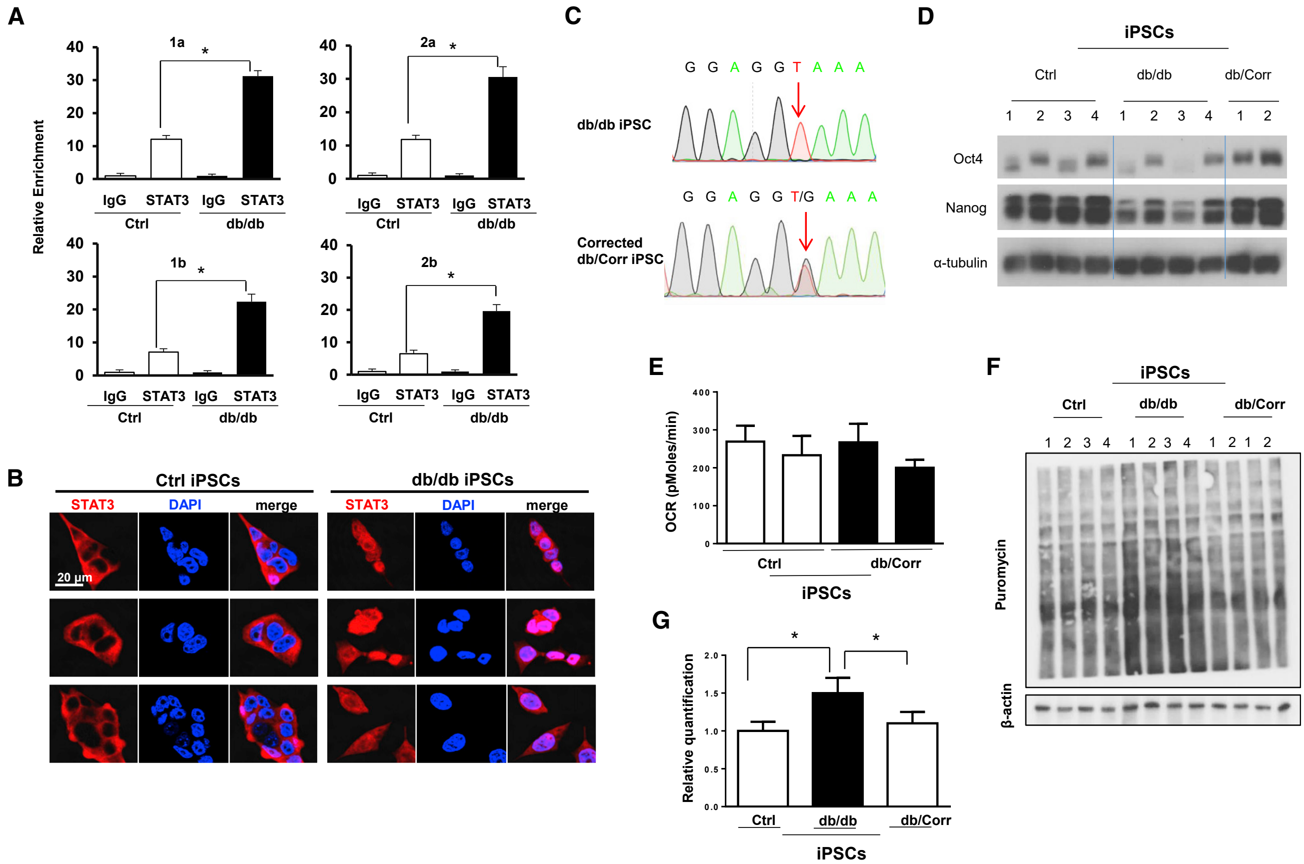

Figure 3. Chromatin Immunoprecipitation Analysis for *Stat3-Eif4e* Binding and CRISPR Correction of the db/db Mutation in iPSCs
(A–E) (A) Chromatin immunoprecipitation analysis showing higher Stat3 binding (relative enrichment) on the two promoter regions "a" and "b" of *Eif4e* in db/db iPSCs using four different sets of primers 1a, 1b and 2a, 2b. (B) Live-confocal microscopy reveals the predominant nuclear localization of STAT3 in db/db iPSCs compared with cytosolic localization of STAT3 in Ctrl iPSCs. Scale bar, 20 μm. Each row indicates a single clone from Ctrl and db/db iPSCs. (C) db/db mutation (G to T) in the intronic region between exon 18 and exon 19, and DNA sequencing reveals the reversal of one copy to wild type in db/db iPSCs. Similar results were obtained in two additional clones. (D) Western blot analysis showing restoration of protein abundance of OCT4 and NANOG in CRISPR-corrected (db/Corr) iPSCs. α-Tubulin was used as a loading control. (E) Metabolic profiling showed similar basal respiration in db/db-corrected iPSCs compared with Ctrl iPSCs.
(F and G) (F) Anti-puromycin western blot analysis showing normalization of protein synthesis in CRISPR-corrected db/Corr iPSCs. β-Actin was used as a loading control. (G) Quantification of data from experiment in (F), n = 3 independent experiments; data are shown as mean ± SD and analyzed by Student's t test (*p < 0.05, **p < 0.01).

and observed a higher polysome/monosome ratio in db/db iPSCs suggesting enhanced protein synthesis (Figures 2F and 2G). These data were confirmed by an alternative non-radioactive approach (Schmidt et al., 2009) wherein addition of puromycin to a growing culture of Ctrl or db/db iPSCs led to increased protein synthesis in the latter at the end of 48 h (Figures 2H and 2I). *In silico* analysis revealed two Stat3 binding regions on the promoter of the *Eif4e* gene, which might be involved in cellular protein synthesis (Figure S5A). Indeed, chromatin immunoprecipitation (ChIP) analysis by real-time PCR, to validate binding of *Stat3* to the promoter of *Eif4e*, showed significantly greater enrichment of *Stat3* binding on the *Eif4e* promoter region in db/db iPSCs as compared with Ctrl iPSCs. The relative enrichment of two *Stat3* binding regions (region 1: from −841 to −834; region 2: from −168 to −160) on the promoter of *Eif4e* were achieved by using 2 pairs of primers to examine each region (1a, 1b for "GGCTTCCC" and 2a, 2b for "TTCCCAGAA") in real-time PCR analysis (Figures 3A and S5B). Moreover, live immunostaining showed predominantly nuclear localization of STAT3 in db/db iPSCs even in the basal state (Figure 3B). Together, these results implicate a role for *Stat3* in the regulation of protein synthesis via *Eif4e* in db/db iPSCs.

CRISPR-Cas9 Correction of db/db iPSCs Normalizes Altered Protein Synthesis and Pluripotency Pathways

To determine whether the mutation in the OB-R is directly relevant for the phenotypes observed in the iPSCs, we designed guide RNAs to target and correct the G to T point mutation using CRISPR-Cas9 genome editing. A control template with the wild-type sequence was used to replace the mutation (Figure S6A). Among the 192 clones selected for sequencing we identified two clones with one copy reverted to the wild-type sequence (db/+), hereafter termed db/Corr iPSCs (Figures 3C and S6B). To examine the effect of the db/db mutation, we performed molecular and functional analysis of Ctrl and CRISPR-corrected (db/Corr) iPSCs. Western blot analysis showed that db/Corr iPSCs exhibited EIF4E and OCT4 protein expression that was similar to Ctrl iPSCs in the basal state (Figures 3D and S6C). Furthermore, metabolic profiling demonstrated similar levels of OCR in the mutation db/Corr iPSCs and Ctrl iPSCs (Figure 3E). Anti-puromycin antibody-based Western blot analyses also revealed that protein synthesis in CRISPR-corrected db/Corr iPSCs is not significantly different from Ctrl iPSCs (Figures 3F and 3G).

RNA-Seq Analyses of iPSCs Authenticate the Role of OB-R in Protein Synthesis and Pluripotency Pathways

To confirm our previous findings, we conducted RNA-seq analyses on Ctrl, db/db, and db/Corr iPSCs. A total of 1,662 upregulated and 1,887 downregulated genes were determined between Ctrl and db/db iPSCs with false discovery rate < 0.25 and adjusted p value < 0.05. This included 651 upregulated genes and 630 downregulated genes between db/db versus Ctrl and db/Corr versus Ctrl iPSCs. Gene ontology and pathway analyses between Ctrl and db/db iPSCs showed an upregulation in the ERK and EIF pathways and downregulation in insulin secretion, alanine-glutamate metabolism, and tyrosine metabolic pathways (Figures 4A and 4B). Heatmaps confirmed the proteomics data with an upregulation of genes related to the protein synthesis machinery (Figures 4C and 5A), while pluripotency-associated genes were downregulated (Figures 4D and 5B) in db/db iPSCs. These alterations were reversed in db/Corr iPSCs.

Volcano plots between db/db versus Ctrl iPSCs revealed the top differentially regulated genes of OB-R in the pluripotent state (Figure 4E; Table S6). Validation studies using real-time PCR analyses confirmed the changes in several genes, including an upregulation of *Eif4e*, *Eif1ax*, caveolae-associated protein 4 (*Cavin4*), and fatty acid binding protein 3 (*Fabp3*), and downregulation of solute carrier family 29, member 3 (*Slc29a3*), tripartite motif-containing 44 (*Trim44*), and transmembrane protein 132c (*Tmem132c*) genes in db/db iPSCs. Again, the differential regulation was normalized in db/Corr iPSCs (Figure 5C).

Directed Differentiation of iPSCs Reveals a Role for OB-R Signaling in Development of the Neuronal Lineage

To investigate the role of leptin receptor signaling in tissues originating from the ectoderm we directed the differentiation toward the neuronal lineage (Gupta et al., 2018; Ying et al., 2003). After differentiation of the iPSCs, we observed downregulation of the neural progenitor markers *Noggin* and *Nestin*, while *Tubb3*+ did not show significant changes at the transcript level on day 15 in the db/db as compared with Ctrls (Figure 5D). Immunostaining analyses confirmed the decrease in NOGGIN+ cells (58.5%; $p < 0.0001$, n = 4) and glial fibrillary acidic protein (GFAP)+ cells (45.5%; p = 0.0019, n = 4) in db/db compared with Ctrl-derived neuronal cells. NESTIN+ cells were decreased in the db/db iPSC-derived neurons (5.4%, p = 0.07, n = 3) as compared with Ctrl neurons (Figures 5E–5H). Morphological images were taken at day 15 differentiated neuronal cells from Ctrl, db/db, and db/Corr iPSCs (Figure 6A). Despite a relatively small decrease in cell numbers we confirmed a decrease in NESTIN protein in db/db neuronal cells by western blot ($\sim$45%; $p < 0.05$, n = 4) and flow cytometry analysis (52.1%; $p < 0.0001$, n = 3; decrease in mean fluorescent intensity) as compared with Ctrl neurons (Figures 6B–6D). The decrease in NOGGIN+ cells was also confirmed by flow cytometry analysis (60.3%; $p < 0.0001$, n = 3) in db/db neurons as compared with Ctrl neurons (Figure 6E). Importantly, the changes in expression of neuronal markers were normalized in db/Corr neurons that were differentiated after correction using CRISPR-Cas9. These results provide direct evidence that defects in leptin receptor signaling prompts mouse iPSCs to reduced/delayed differentiation toward the ectodermal lineage.

DISCUSSION

db/db mice that manifest impaired leptin signaling are widely used as a disease model (Bates et al., 2005; Ernst et al., 2013). These homozygous mutant mice are born normally but develop diabetes and metabolic abnormalities at $\sim$6–8 weeks of age characterized by mitochondrial dysfunction (Holmstrom et al., 2012; Wang et al., 2014) while the heterozygous mice are relatively normal (Kobayashi et al., 2000). We report, for the first time, metabolic dysfunction and upregulated MEK/ERK pathways in the db/db embryonic fibroblasts that were morphologically larger and exhibited greater glycolytic and OX/PHOS capacities.

We used a proteomics approach and confirmed altered expression of OCT4 and EIF4E protein synthesis pathways in the db/db iPSCs. These observations have significant implications since OCT4 and NANOG are known to play key

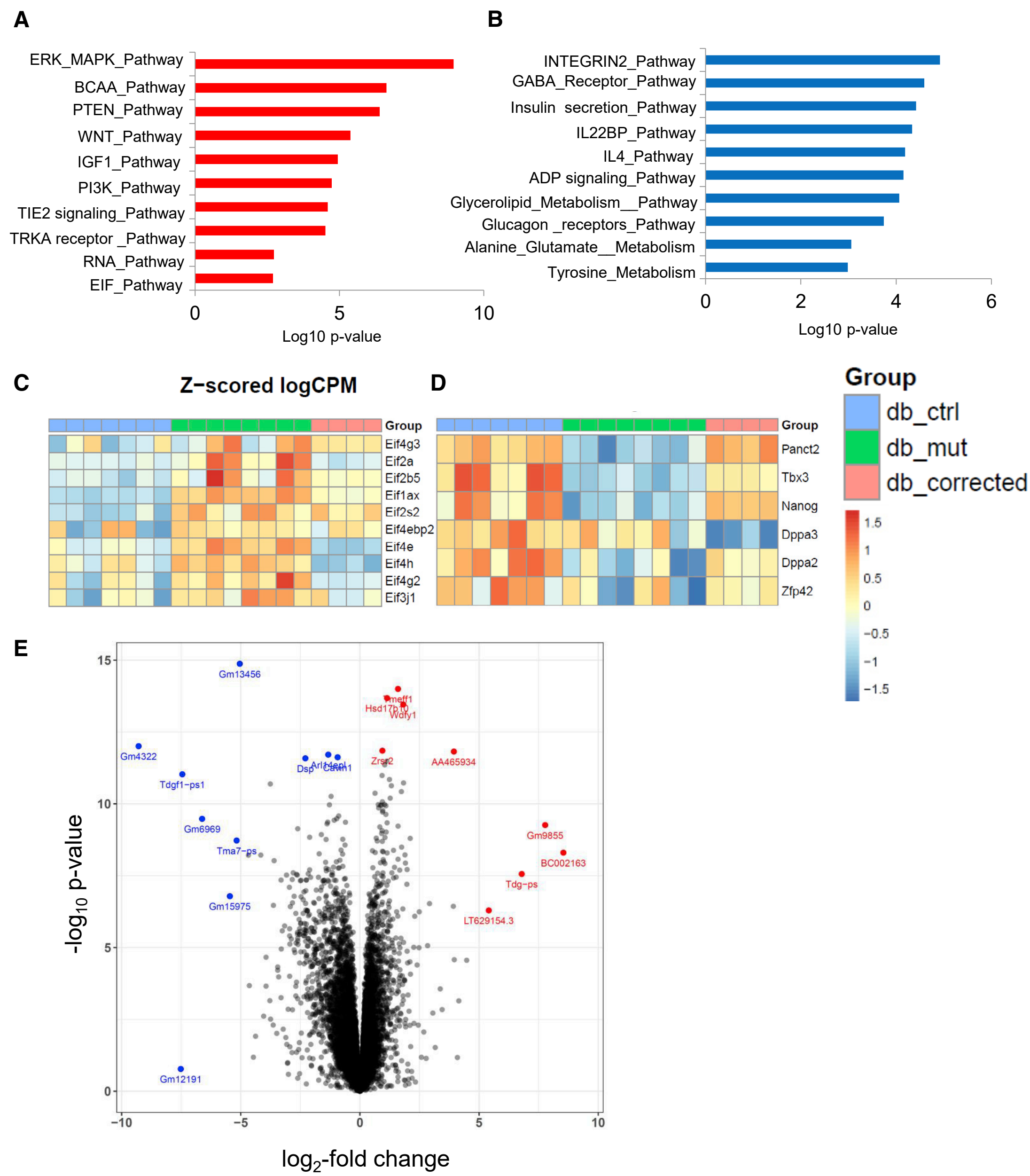

Figure 4. RNA-Seq Analyses Confirms Upregulation of Protein Synthesis Pathways and Downregulation of Pluripotency-Associated Genes

(A–C) Red color indicates upregulated pathways (A) and blue color indicates downregulated pathways (B) in db/db iPSCs as compared with Ctrl iPSCs. (C) Several genes related to protein synthesis pathways were upregulated in db/db iPSCs and were normalized after CRISPR-Cas9 correction of iPSCs.

(D) Pluripotency genes were downregulated in db/db iPSCs.

(E) Volcano plot showing differentially regulated genes between Ctrl and db/db iPSCs. Red color indicates genes that are upregulated and blue color indicates downregulated genes in db/db iPSCs as compared with Ctrl iPSCs. n = 3 independent experiments; data are shown as mean ± SD and analyzed by Student's t test (*$p < 0.05$, **$p < 0.01$).

roles in maintaining pluripotency of iPSCs (Boiani et al., 2002; Chambers et al., 2003) and a quantitative change in the expression of *Oct4* leads to differentiation, de-differentiation, or self-renewal of iPSCs (Niwa et al., 2000). Interestingly, RNA-seq analyses demonstrated that the expression of *Nanog*, *Tbx3*, *Panct2*, and *Zfp42* were all decreased

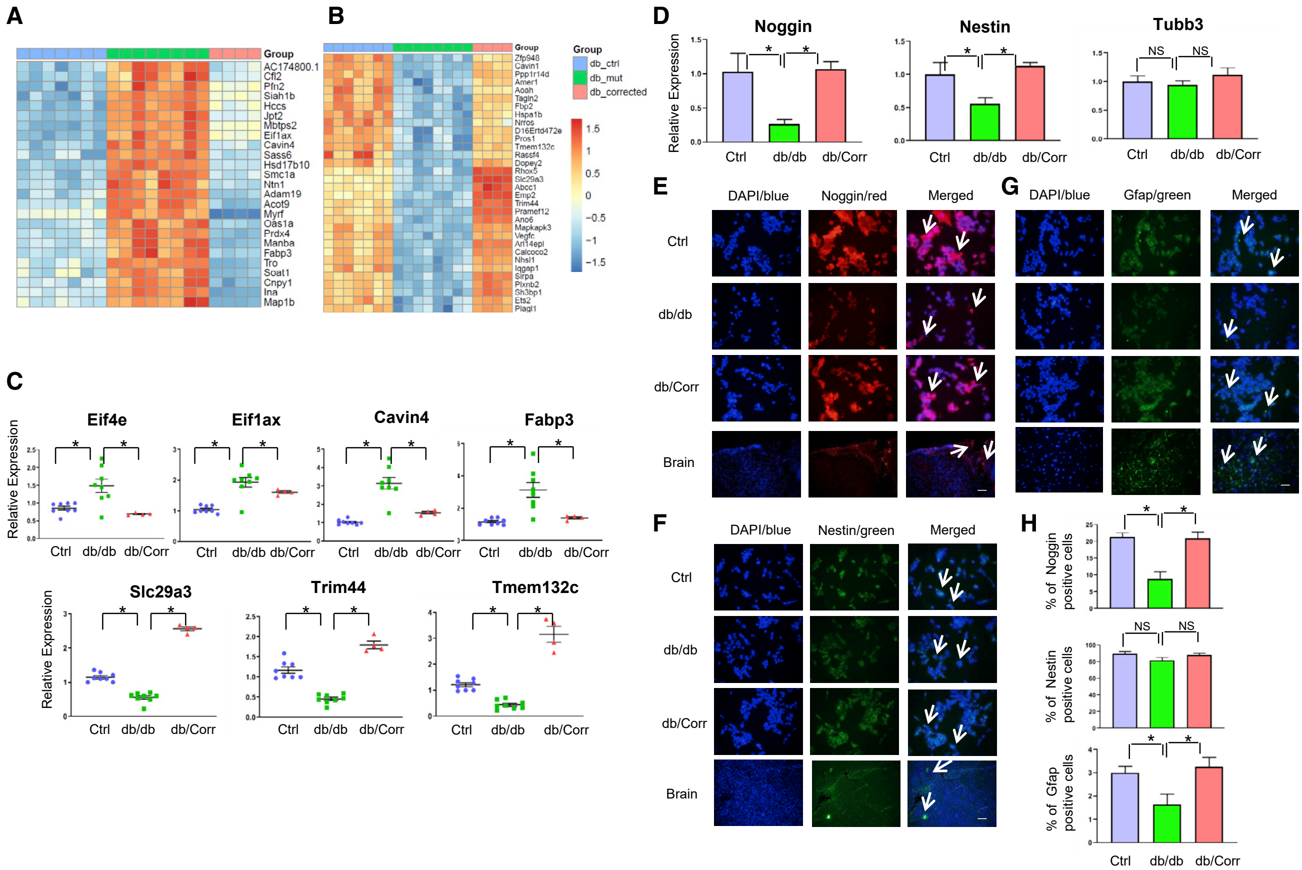

Figure 5. Neuronal Differentiation of Ctrl, db/db, and db/Corr iPSCs Points to a Role for Leptin Receptors in the Regulation of Early Neuronal Markers

(A) Heatmap analyses showing upregulation of top differentially regulated genes in db/db iPSCs that were normalized in db/Corr iPSCs.
(B) Heatmap analyses showing downregulation of top differentially regulated genes in db/db iPSCs that were normalized in db/Corr iPSCs. Genes in red color denote upregulation while genes in blue color represent downregulation. Pathway analyses were conducted using Limma pathway software.
(C) Real-time PCR analyses of *Eif4e*, *Eif1ax*, *Cavin4*, *Fabp3* (upregulated in db/db iPSCs), and *Slc29a3*, *Trim44*, *Tmem132c* (downregulated in db/db iPSCs) as a comparison with Ctrl iPSCs. Expression of these genes was normalized in corrected db/Corr iPSCs. β-Actin was used as a loading control. Gene expression in blue indicates Ctrl iPSCs, in green indicates db/db iPSCs, and in red indicates corrected db/Corr iPSCs.
(D) Real-time PCR analyses of early neuronal markers *Noggin*, *Nestin*, and *Tubb3* in total RNA from day 15 neuronal cells.
(E–G) Representative images of Ctrl, db/db, and db/corr iPSC-derived neuronal cells (day 15) immunostained for markers of neuronal cells (E) NOGGIN (in red), (F) NESTIN (in green), and (G) GFAP (in green). All nuclei were stained in blue with DAPI. Mouse brain tissue was used as positive control. Scale bar, 100 μm.
(H) At least four independent images of each marker were quantified by manual counting. The percent of positive cells of each neuronal marker was determined by counting approximately 1,000 nuclei/image. n = 3 independent experiments; data are shown as mean ± SD and analyzed by Student's t test (*p < 0.05, **p < 0.01).

in db/db iPSCs, while the *Oct4* transcript levels did not change. One interpretation of the latter observation is that OB-R is involved in post-transcriptional regulation of OCT4 at the pluripotent stage. Nevertheless, the reduced abundance of OCT4, NANOG, and other pluripotency markers in the db/db iPSCs suggests a potential impact on the differentiation process.

The translation initiation factor, eIF4e, has been reported to play an important role in protein synthesis and cell growth (Gingras et al., 1999; Sonenberg and Gingras, 1998). Our data indicate that disruption of OB-R leads to enhanced protein synthesis likely due persistent activation of *Stat3* binding to the promoter of *Eif4e* in db/db iPSCs as shown by ChIP analysis and immuno-staining. While these observations may appear contradictory to previous reports of leptin stimulating protein synthesis in human trophoblast cells (Perez-Perez et al., 2009), and leptin acting via the OB-R to promote Stat3 phosphorylation and

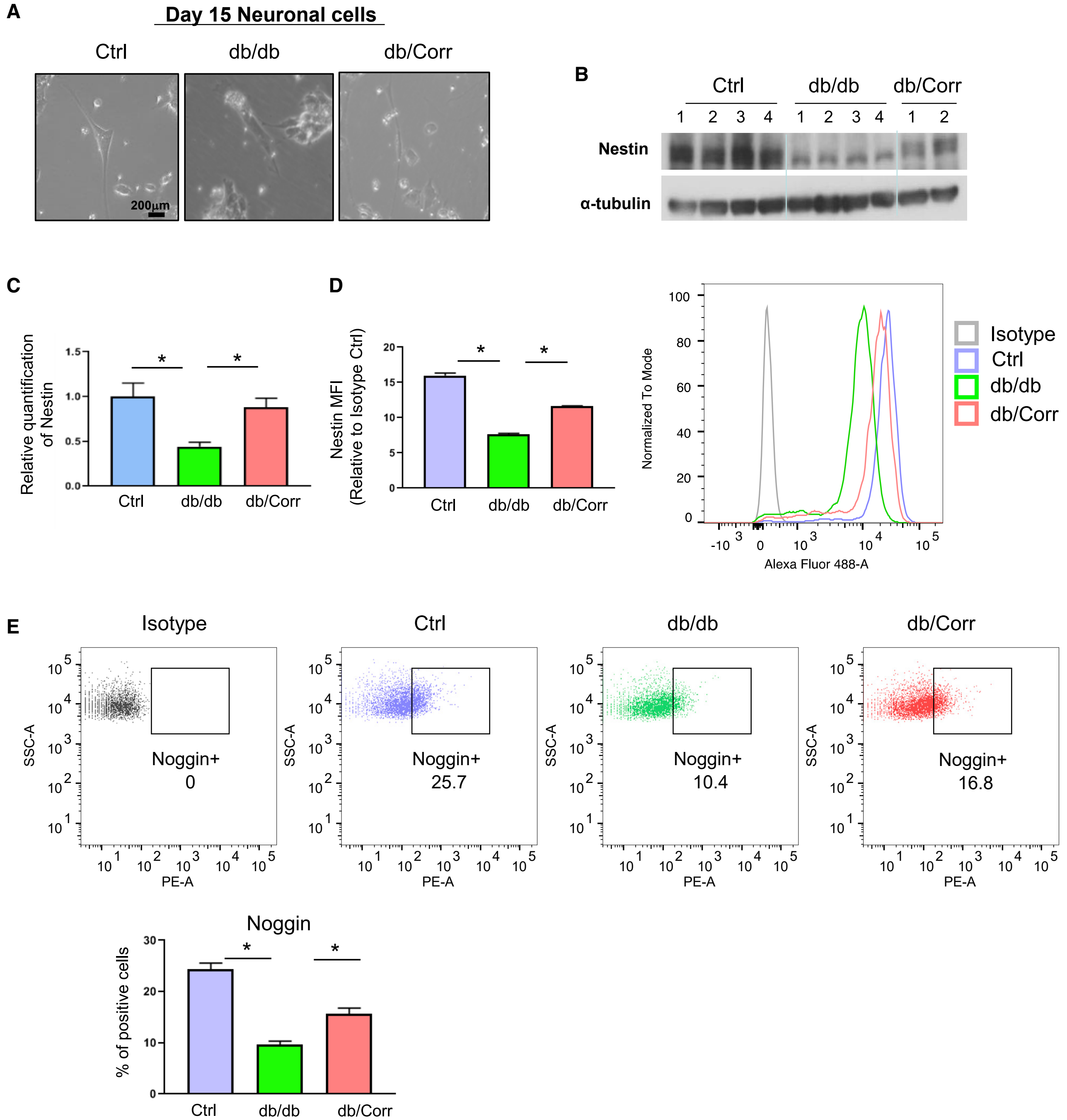

Figure 6. Neuronal Differentiation of db/Corr iPSCs Shows the Ability of Gene Editing to Restore the Defects in Regulation of Early Neuronal Markers

(A) Morphological images of cells on day 15 of directed differentiation of Ctrl, db/db, or db/+ iPSCs. Scale bar, 200 μm.

(B) Total protein was isolated from day 15 differentiated neuronal cells. NESTIN antibody was used to detect its abundance in day 15 neuronal cells from Ctrl, db/db, or db/Corr groups. α-Tubulin was used as housekeeping control as shown in representative western blot.

(C and D) (C) Quantification of NESTIN western blot using ImageJ software. (D) NESTIN mean fluorescent intensity measurement of Ctrl, db/db, and db/Corr iPSC differentiated neuronal cells by flow cytometry.

(E) Flow cytometry analyses of NOGGIN+ cells from differentiated neuronal cells of Ctrl, db/db, and db/Corr iPSCs.

n = 3 independent experiments; data are shown as mean ± SD and analyzed by Student's t test (* $p < 0.05$, ** $p < 0.01$).

nuclear translocation in tumor initiating stem cells (Feldman et al., 2012), it is possible that leptin-activated Stat3 has context-dependent effects during the pluripotent stage. Furthermore, one cannot exclude the possibility of MEK/ERK pathways in activating EIF4E protein synthesis, similar to the effect of leptin on human trophoblast cell lines, in db/db iPSCs.

The successful restoration of metabolic function, pluripotency genes, and protein synthesis after correction of the db/db mutation (G to T) on one allele in db/Corr iPSCs using CRISPR-Cas 9 genome editing (Hsu et al., 2014) confirms a direct role for OB-R in maintenance of pluripotency and cell differentiation processes. The RNA-seq data on iPSCs confirms the observations after gene correction of OB-R with normalization of expression of several genes including *Eif4e*, *Eif1ax* to the level observed in Ctrl iPSCs.

Consistent with the report of leptin signaling being linked to neuronal embryonic development (Croizier et al., 2016), we observed a decrease in NOGGIN and GFAP+ cells and reduction in NESTIN protein, on day 15 of neuronal differentiation of db/db iPSCs. These changes were normalized in neuronal cells obtained from CRISPR-corrected db/Corr iPSCs. Mice lacking NOGGIN have been reported to develop defects in hypothalamic patterning, which is important for maintaining energy homeostasis during adulthood (Davis and Camper, 2007). Thus, in this scenario, and based on our findings, it is plausible that a decrease in NOGGIN+ cells in db/db mice during development leads to impaired development of POMC and AgRP neurons with consequences on development of obesity, diabetes, and metabolic syndrome as the mouse attains adulthood. Nestin has been reported to be important for self-renewal of neural progenitor cells and axonal growth of neurons (Bott et al., 2019) and its deficiency has been linked to impaired motor coordination (Mohseni et al., 2011). In our study, the reduction in Nestin protein could affect the neuronal projections/axonal growth that would in turn lead to impairment of normal neuronal development and coordination during adulthood.

Notably, previous studies by Ramos-Lobo et al. (2019) reported reduced Gfap expression in the hypothalamus of LepR null mice during early life with long-term consequences. Another study reported that modulation of Gfap-expressing glial cells in the hypothalamus is able to regulate feeding (Chen et al., 2016). In the context of these reports, the reduction in GFAP+ cells in db/db neuronal cells, as compared with Ctrl and db/Corr neurons, in our own study, argues for a potential reduction in GFAP+ glial cells in the hypothalamus with implications for feeding behavior. Our studies also gain significance since metabolic defects in the db/db mice, in contrast to the ob/ob model, cannot be fully restored by treatment with exogenous leptin (Pellymounter, 1995; Harris, 2001). Taken together, our findings indicate that normal leptin receptor expression and signaling regulates neural stem cell markers (e.g., NOGGIN and NESTIN) and GFAP protein during early developmental stages, which is necessary for maintenance of normal structural and/or functional properties of neurons populating the hypothalamus with implications for development of metabolic disorders in adulthood.

In summary, we report defects in MEFs and iPSCs derived from db/db mice with several implications. First, the regulation of *Nanog*, *Tbx3*, and *Zfp42* at the transcript level and OCT4, and NANOG at the protein level in cells with the db/db mutation suggests a role for leptin signaling in regulation of "stemness." Second, linking db/db signaling to protein synthesis pathways via the Stat3/Eif4e axis in iPSCs provides insights in understanding the incidence of cancer in leptin receptor dysfunctional states. Third, a decrease in the stem cell markers NOGGIN, NESTIN, and GFAP during directed differentiation of db/db iPSCs suggests a role for OB-R signaling in the regulation of neuronal development. Thus, db/db MEFs and iPSCs provide useful tools (depicted in the Graphical Abstract) to explore the relevance of OB-R in the early origins of obesity, diabetes, and metabolic abnormalities, and to find putative targets for harnessing therapeutics to prevent the development of these diseases.

EXPERIMENTAL PROCEDURES

Mice and MEFs

All studies involving mice were approved by the institutional review board of the Joslin Diabetes Center and were in accordance with NIH guidelines. Embryonic day 14.5 wild-type control (Ctrl) (N = 4) and db/db MEFs (N = 4) were derived from breeding OB-R$^{db/+}$ heterozygous mice (Jackson Laboratory). All fibroblasts were maintained up to a maximum passage ~10 in Dulbecco modified Eagle's medium supplemented with GlutaMAX, 10% fetal bovine serum (FBS), and 1% nonessential amino acids.

Lentiviral-Mediated Reprogramming and iPSC Generation and Characterization

Generation of mouse iPSCs involved infection of primary MEFs with mouse STEMCCA lentivirus vector expressing the reprogramming factors *Oct4*, *Sox2*, *Klf4*, and *cMyc*. iPSC characterization involved teratoma formation, H&E staining, and immunostaining for the three lineage markers staining performed according to previous reports (Bhatt et al., 2015; Sommer et al., 2009; Teo et al., 2013). More information is available in the Supplemental material.

Gene Expression Analyses Using Quantitative RT-PCR and Western Immunoblotting

RNA was isolated from cells using RNeasy kit (QIAGEN) and cDNA was prepared from 1 μg of RNA using the RT-PCR kit (Life Technologies) according to the manufacturer's instructions and diluted to a final volume of 250 μL. In parallel experiments total cellular proteins were harvested using M-PER mammalian protein extraction reagent (Thermo Scientific) followed by western immunoblotting of proteins. More information about antibodies is included in Supplemental material.

Gene Correction in db/db iPSCs Using CRISPR-Cas9

The Cas9 and sgRNA plasmid *pX459* were obtained from Addgene (plasmid no. 48139). Guide RNAs (20 bps) were chosen that lie in the intronic region between exons 18 and 19 of the OB-R gene using the CRISPR Design Tool (http://crispr.mit.edu/). The sequence of sgRNA cloned in vector was CACCGGATGTTTACATTTTGATGG (sgRNA-01), and a 200-nt DNA oligo complementing the region was used as repair template (seq CACTCTTTGAAGTCTCTCAT GACCACTACAGATGAACCCAATCTACCAACTTCCCAACAGTCC ATACAATATTAGAAGATGTTTACATTTTGATGGAGGGAAACAAAC CTAAACTATGGTTTGAATGACTAAGAAATAACATTTGATGAGCT TATTAGAGAAGTGTATATTTTGTGGCCACAATGTAGGTTTGATG TAGT, purchased as ssODN Ultramer Oligo from IDT). db/db iPSCs cells were electroporated using 500 ng of vector and 50 pmol of ssODN template using Amaxa Nucleofector (cat. no. VAPH-1001, Nucleofector Program A-23). Cells were plated on a 15-cm dish and, after overnight culture, 50 ng/mL of puromycin selection was applied for the first 2 days of culture. Colonies started appearing within 5–7 days and individual colonies/clones were manually picked and transferred to 48-well plates.

Genotyping for 100 clones was performed by extracting genomic DNA (PureLink Genomic DNA Kit, Thermo Fischer Scientific) that was subjected to PCR (using F primer TCTCTGAATCCTTGCTC TTTGT, R primer CATGTGGTTGCTGGGATTTG) followed by Sanger sequencing using sequencing primer CCCTCTCCTAA GTGTGTCACTA. Data from sequencing traces were analyzed using SeqmanPro software (Lasergene SeqMan Pro version 8.1; DNASTAR). Clones with and without gene correction were compared for *in vitro* studies (isogeneic pair). In addition the clones were analyzed for potential off-target effects for top predicted off-target sites (NCBI-BLAST) using the Sanger sequencing method.

Flow Cytometry

iPSCs derived from Ctrl and db/db MEFs were trypsinized using 0.05% trypsin-EDTA. Single cells were stained for Mito-GFP dye with proper isotype controls using methods described previously (Gupta et al., 2015). For neuronal marker staining, cells were harvested and fixed in 4% paraformaldehyde for 15 min at room temperature. Cells were then spun and washed with cold fluorescence-activated cell sorting (FACS) buffer (5% FBS in PBS). Permeabilization and blocking was carried out on ice for 30 min in FACS buffer with 0.1% Triton X-100. Antibody staining was performed on ice for 30 min using chicken anti-NESTIN (1:100, NB100-1604; Novus Biologicals), rabbit anti-NOGGIN (1:50, ab-16054, Abcam) followed by incubation with secondary antibody (anti-chicken Alexa 488 and anti-rabbit Alexa 594; 1:1,000, Invitrogen) for 30 min on ice. Cells were washed and resuspended in 250 μL FACS buffer and filtered through a 30-μm filter before analysis by LSR II (BD Biosciences, Joslin Flow Cytometry Core). Gating was determined according to the secondary-only controls.

Metabolic Profiling

Bioenergetic profiles of MEFs and mouse iPSCs were generated using a Seahorse Bioflux Analyzer as reported earlier (Kleinridders et al., 2013). The brief method is described in the Supplemental material.

Chromatin Immunoprecipitation and Immunofluorescence

In brief, Ctrl and db/db iPSCs were fixed in 1% formaldehyde, and quenched in glycine. Cells were washed with PBS and lysed in cold lysis buffer with protease and phosphatase inhibitors (Sigma). Cells were then sonicated using 25% of power, 10-s on/off pulses for a total of 3 min. Immunoprecipitations were performed using anti-STAT3 antibody (Santa Cruz). Ctrl and db/db iPSCs were transferred onto poly-L-lysine pre-coated cover slips and incubated at 37°C for 24 h. Cells on cover slips were fixed with 2% formaldehyde and stained with anti-STAT3 antibody followed by anti-rabbit IgG Alexa 594 (Molecular Probes). Cover slips were mounted with Fluorescent Mounting Media (DAKO) and cells were analyzed under a Carl Zeiss LSM7 confocal laser scanning microscope.

Immunohistochemistry

Neuronal cells grown on glass slides were fixed in 4% paraformaldehyde solution (Wako) before staining with specific primary antibodies as described previously. More information is available in the Supplemental material.

Mass Spectrometry Analyses

We generated biological replicates for each of the db/db and Ctrl mouse cell cultures, both before (i.e., from MEFs; n = 2 + 2 replicates) and after reprogramming (i.e., from iPSCs; n = 4 + 4 replicates) as outlined in Figure S2. Subsequently, the eight iPSC and four MEF cell lines were multiplexed by isobaric labeling and subjected to independent liquid chromatography-mass spectrometry analysis as described in the Supplemental material.

RNA-Seq Analyses

We isolated total RNA from Ctrl (N = 4), db/db (N = 4), and db/Corr (N = 2) iPSCs in duplicates and sent it out to DNA Link for sequencing. RNA-seq data were analyzed in the Joslin Bioinformatic core facility. RNA-seq raw reads were downloaded from DNA Link, which were reverse stranded paired-end reads. There were 14,245 genes after filtering out the low expressing genes. We then normalized counts by weighted trimmed mean of M values. The normalization factors were between 0.93 and 1.08. Detailed methods for analyses are described in the Supplemental material.

Neuronal Differentiation

Fifty thousand Ctrl, db/db, and db/Corr iPSCs were plated on gelatin-coated six-well plates and differentiated up to 15 days in NDiff 227 medium (Clontech). Cells were harvested on day 15 for transcript and western blot analyses for neuronal markers.

Data and Code Availability

The accession number for the RNA-seq data reported in this paper is GSE155704 proteomics data reported in this paper via ProteomeXchange with identifier is PXD020959.

SUPPLEMENTAL INFORMATION

Supplemental Information can be found online at https://doi.org/10.1016/j.stemcr.2020.10.001.

AUTHOR CONTRIBUTIONS

M.K.G. conceived and designed the experimental study, and wrote the manuscript. H.V., S.S., T.N.R., V.W., J.S., H.B., M.V., T.T., S.K., M.S., R.M., J.H., and Y.B. performed the experiments and analyzed the data. H.R. supervised the study and edited the manuscript. R.N.K. conceived, designed, and supervised the study, provided funding and resources, and edited the manuscript. All authors read and agreed on manuscript.

ACKNOWLEDGMENTS

We thank G. Mostoslavsky PhD (Boston University) for the kind gift of STEMCCA lentiviral plasmids and C.R. Kahn MD (Joslin Diabetes Center) for the use of the Seahorse instrument. We thank D.M. Smith PhD (Astra Zeneca) and B. Tyberg PhD (Astra Zeneca) for support and discussions, and G. Daley MD PhD (Children's Hospital, Boston) for discussions. The authors acknowledge Jonathan Dreyfuss and Hui Pan from Joslin Bioinformatics Core facility for RNA-seq analyses. The authors also acknowledge the iPSC Core Facility (DRC, NIH P30 DK036836), and C. Cahill for assistance with electron microscopy (Advanced Microscopy Facility DRC, NIH DK036836). M.K.G. is supported by a JDRF Advanced Postdoctoral Fellowship Award 3-APF-2017-393-A-N. S.S. is supported by NIH K12 HD000850, P30 DK40561, and NASPGHAN Young Investigator/Nestle Nutrition Award. J.S. is supported by a grant from SICORP of AMED with A*STAR. R.N.K. acknowledges support from R01 DK67536 and R01 DK103215 and a grant from AstraZeneca. S.S is supported by NIH K12 HD000850. T.N.R. is supported by a grant from the Swiss National Science Foundation (320030_189090/1). H.B. and H.R are supported by The Bergen Research Foundation (Bergen Forskningsstiftelse); H.R. is supported by Novo Nordisk Fonden and Western Norway Regional Health Authority.

Received: July 18, 2019
Revised: October 1, 2020
Accepted: October 1, 2020
Published: October 29, 2020

REFERENCES

Anisimov, S.V., Christophersen, N.S., Correia, A.S., Hall, V.J., Sandelin, I., Li, J.Y., and Brundin, P. (2011). Identification of molecules derived from human fibroblast feeder cells that support the proliferation of human embryonic stem cells. Cell Mol. Biol. Lett. *16*, 79–88.

Bates, S.H., Kulkarni, R.N., Seifert, M., and Myers, M.G., Jr. (2005). Roles for leptin receptor/STAT3-dependent and -independent signals in the regulation of glucose homeostasis. Cell Metab. *1*, 169–178.

Bhatt, S., Gupta, M.K., Khamaisi, M., Martinez, R., Gritsenko, M.A., Wagner, B.K., Guye, P., Busskamp, V., Shirakawa, J., Wu, G., et al. (2015). Preserved DNA damage checkpoint pathway protects against complications in long-standing type 1 diabetes. Cell Metab. *22*, 239–252.

Boiani, M., Eckardt, S., Scholer, H.R., and McLaughlin, K.J. (2002). Oct4 distribution and level in mouse clones: consequences for pluripotency. Genes Dev. *16*, 1209–1219.

Bott, C.J., Johnson, C.G., Yap, C.C., Dwyer, N.D., Litwa, K.A., and Winckler, B. (2019). Nestin in immature embryonic neurons affects axon growth cone morphology and Semaphorin3a sensitivity. Mol. Biol. Cell *30*, 1214–1229.

Chambers, I., Colby, D., Robertson, M., Nichols, J., Lee, S., Tweedie, S., and Smith, A. (2003). Functional expression cloning of Nanog, a pluripotency sustaining factor in embryonic stem cells. Cell *113*, 643–655.

Chen, H., Charlat, O., Tartaglia, L.A., Woolf, E.A., Weng, X., Ellis, S.J., Lakey, N.D., Culpepper, J., Moore, K.J., Breitbart, R.E., et al. (1996). Evidence that the diabetes gene encodes the leptin receptor: identification of a mutation in the leptin receptor gene in db/db mice. Cell *84*, 491–495.

Chen, N., Sugihara, H., Kim, J., Fu, Z., Barak, B., Sur, M., Feng, G., and Han, W. (2016). Direct modulation of GFAP-expressing glia in the arcuate nucleus bi-directionally regulates feeding. eLife *5*. https://doi.org/10.7554/eLife.18716.

Clement, K., Vaisse, C., Lahlou, N., Cabrol, S., Pelloux, V., Cassuto, D., Gourmelen, M., Dina, C., Chambaz, J., Lacorte, J.M., et al. (1998). A mutation in the human leptin receptor gene causes obesity and pituitary dysfunction. Nature *392*, 398–401.

Croizier, S., Prevot, V., and Bouret, S.G. (2016). Leptin controls parasympathetic wiring of the pancreas during embryonic life. Cell Rep. *15*, 36–44.

Davis, S.W., and Camper, S.A. (2007). Noggin regulates Bmp4 activity during pituitary induction. Dev. Biol. *305*, 145–160.

El-Hefnawy, T., Ioffe, S., and Dym, M. (2000). Expression of the leptin receptor during germ cell development in the mouse testis. Endocrinology *141*, 2624–2630.

Ernst, A., Sharma, A.N., Elased, K.M., Guest, P.C., Rahmoune, H., and Bahn, S. (2013). Diabetic db/db mice exhibit central nervous system and peripheral molecular alterations as seen in neurological disorders. Transl. Psychiatry *3*, e263.

Feldman, D.E., Chen, C., Punj, V., Tsukamoto, H., and Machida, K. (2012). Pluripotency factor-mediated expression of the leptin receptor (OB-R) links obesity to oncogenesis through tumor-initiating stem cells. Proc. Natl. Acad. Sci. U S A *109*, 829–834.

Ghilardi, N., Ziegler, S., Wiestner, A., Stoffel, R., Heim, M.H., and Skoda, R.C. (1996). Defective STAT signaling by the leptin receptor in diabetic mice. Proc. Natl. Acad. Sci. U S A *93*, 6231–6235.

Gingras, A.C., Raught, B., and Sonenberg, N. (1999). eIF4 initiation factors: effectors of mRNA recruitment to ribosomes and regulators of translation. Annu. Rev. Biochem. *68*, 913–963.

Gupta, M.K., De Jesus, D.F., Kahraman, S., Valdez, I.A., Shamsi, F., Yi, L., Swensen, A.C., Tseng, Y.H., Qian, W.J., and Kulkarni, R.N. (2018). Insulin receptor-mediated signaling regulates pluripotency markers and lineage differentiation. Mol. Metab. *18*, 153–163.

Gupta, M.K., Teo, A.K., Rao, T.N., Bhatt, S., Kleinridders, A., Shirakawa, J., Takatani, T., Hu, J., De Jesus, D.F., Windmueller, R., et al. (2015). Excessive cellular proliferation negatively impacts reprogramming efficiency of human fibroblasts. Stem Cell Transl. Med. *4*, 1101–1108.

Harris, R.B., Mitchell, T.D., Yan, X., Simpson, J.S., and Redmann, S.M., Jr. (2001). Metabolic responses to leptin in obese db/db mice are strain dependent. Am J Physiol Regul Integr Comp Physiol https://doi.org/10.1152/ajpregu.2001.281.1.R115.

Hoggard, N., Haggarty, P., Thomas, L., and Lea, R.G. (2001). Leptin expression in placental and fetal tissues: does leptin have a functional role? Biochem. Soc. Trans. *29*, 57–63.

Holmstrom, M.H., Iglesias-Gutierrez, E., Zierath, J.R., and Garcia-Roves, P.M. (2012). Tissue-specific control of mitochondrial respiration in obesity-related insulin resistance and diabetes. Am. J. Physiol. Endocrinol. Metab. *302*, E731–E739.

Hsu, P.D., Lander, E.S., and Zhang, F. (2014). Development and applications of CRISPR-Cas9 for genome engineering. Cell *157*, 1262–1278.

Kleinridders, A., Lauritzen, H.P., Ussar, S., Christensen, J.H., Mori, M.A., Bross, P., and Kahn, C.R. (2013). Leptin regulation of Hsp60 impacts hypothalamic insulin signaling. J. Clin. Invest. *123*, 4667–4680.

Kobayashi, K., Forte, T.M., Taniguchi, S., Ishida, B.Y., Oka, K., and Chan, L. (2000). The db/db mouse, a model for diabetic dyslipidemia: molecular characterization and effects of Western diet feeding. Metabolism *49*, 22–31.

Margetic, S., Gazzola, C., Pegg, G.G., and Hill, R.A. (2002). Leptin: a review of its peripheral actions and interactions. Int. J. Obes. Relat. Metab. Disord. *26*, 1407–1433.

Mohseni, P., Sung, H.K., Murphy, A.J., Laliberte, C.L., Pallari, H.M., Henkelman, M., Georgiou, J., Xie, G., Quaggin, S.E., Thorner, P.S., et al. (2011). Nestin is not essential for development of the CNS but required for dispersion of acetylcholine receptor clusters at the area of neuromuscular junctions. J. Neurosci. *31*, 11547–11552.

Niwa, H., Miyazaki, J., and Smith, A.G. (2000). Quantitative expression of Oct-3/4 defines differentiation, dedifferentiation or self-renewal of ES cells. Nat. Genet. *24*, 372–376.

Pellymounter, M.A., Cullen, M.J., Baker, M.B., Hecht, R., Winters, D., Boone, T., and Collins, F. (1995). Effects of the obese gene product on body weight regulation in ob/ob mice. Science https://doi.org/10.1126/science.7624776.

Perez-Perez, A., Maymo, J., Gambino, Y., Duenas, J.L., Goberna, R., Varone, C., and Sanchez-Margalet, V. (2009). Leptin stimulates protein synthesis-activating translation machinery in human trophoblastic cells. Biol. Reprod. *81*, 826–832.

Ramos-Lobo, A.M., Teixeira, P.D., Furigo, I.C., Melo, H.M., de, M.L.E.S.N., De Felice, F.G., and Donato, J., Jr. (2019). Long-term consequences of the absence of leptin signaling in early life. eLife *8*. https://doi.org/10.7554/eLife.40970.

Saeed, S., Bonnefond, A., Manzoor, J., Philippe, J., Durand, E., Arshad, M., Sand, O., Butt, T.A., Falchi, M., Arslan, M., et al. (2014). Novel LEPR mutations in obese Pakistani children identified by PCR-based enrichment and next generation sequencing. Obesity *22*, 1112–1117.

Schmidt, E.K., Clavarino, G., Ceppi, M., and Pierre, P. (2009). SUnSET, a nonradioactive method to monitor protein synthesis. Nat. Methods *6*, 275–277.

Sommer, C.A., Stadtfeld, M., Murphy, G.J., Hochedlinger, K., Kotton, D.N., and Mostoslavsky, G. (2009). Induced pluripotent stem cell generation using a single lentiviral stem cell cassette. Stem Cells *27*, 543–549.

Sonenberg, N., and Gingras, A.C. (1998). The mRNA 5′ cap-binding protein eIF4E and control of cell growth. Curr. Opin. Cell Biol. *10*, 268–275.

Teo, A.K., Windmueller, R., Johansson, B.B., Dirice, E., Njolstad, P.R., Tjora, E., Raeder, H., and Kulkarni, R.N. (2013). Derivation of human induced pluripotent stem cells from patients with maturity onset diabetes of the young. J. Biol. Chem. *288*, 5353–5356.

Vaisse, C., Halaas, J.L., Horvath, C.M., Darnell, J.E., Jr., Stoffel, M., and Friedman, J.M. (1996). Leptin activation of Stat3 in the hypothalamus of wild-type and ob/ob mice but not db/db mice. Nat. Genet. *14*, 95–97.

Wang, B., Chandrasekera, P.C., and Pippin, J.J. (2014). Leptin- and leptin receptor-deficient rodent models: relevance for human type 2 diabetes. Curr. Diabetes Rev. *10*, 131–145.

Ying, Q.L., Stavridis, M., Griffiths, D., Li, M., and Smith, A. (2003). Conversion of embryonic stem cells into neuroectodermal precursors in adherent monoculture. Nat. Biotechnol. *21*, 183–186.

Stem Cell Reports, Volume *15*

Supplemental Information

Leptin Receptor Signaling Regulates Protein Synthesis Pathways and Neuronal Differentiation in Pluripotent Stem Cells

Manoj K. Gupta, Heidrun Vethe, Samir Softic, Tata Nageswara Rao, Vilas Wagh, Jun Shirakawa, Harald Barsnes, Marc Vaudel, Tomozumi Takatani, Sevim Kahraman, Masaji Sakaguchi, Rachael Martinez, Jiang Hu, Yngvild Bjørlykke, Helge Raeder, and Rohit N. Kulkarni

Figure S1

Supplemental Figures and Legends

A

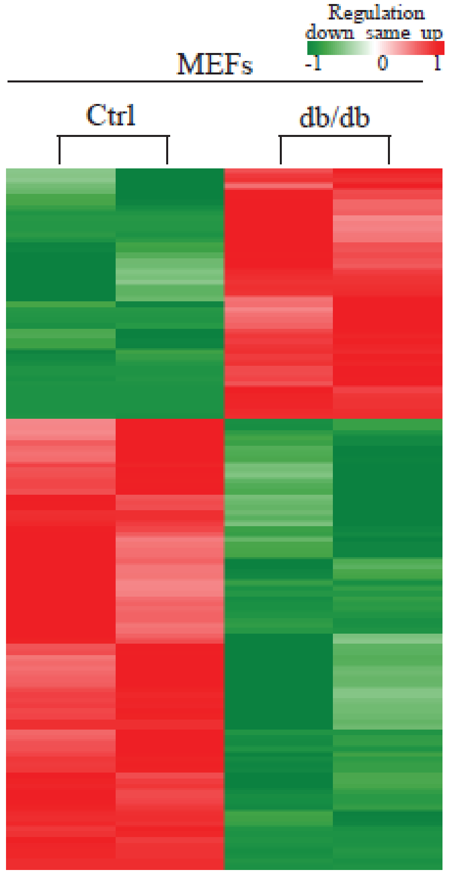

Cellular movement
-ADAM15, CDKN2A, CRMP1,CYR61, DDR2, FST, GBP2, IGFBP7, LOXL2, NCAM1
Cell morphology
-ADAM15, CDKN2A, CRMP1, IGFBP7, LOXL2, TNC
Cell-to-cell signaling interaction
-CRMP1, NCAM1, SYNPO, TNC, VDAC1, VDAC3
Cellular development
-CYR61, FST, CDKN2A, NCAM1, TNC, WLS
Cellular assembly and organization
-CDKN2A, CYR61, VDAC1, NCAM1, SNCG, ADAM15, CYR61, NCAM1, Podxl

Cellular assembly and organization
-ATP5F1D, ATP5MF, ATP5PB, ATP5PO, FHL1, GSN, AUKRA, KIF11
Energy production
-ATP5F1D, ATP5MF, ATP5PB, ATP5PO, CAV1
Nucleic acid metabolism
-ATP5F1D, ATP5MF, ATP5PB, ATP5PO, CAV1, NUCB2, DCK
small molecule biochemistry
-ATP5F1D, ATP5MF, ATP5PB, ATP5PO, CAV1, GM2A, HEXA
cell cycle
-AUKRA, KIF11, ARPC1B, CAV1, DBI, DCK, HDAC1, PARP2

B

Mitochondrial dysfunction

Symbol	Identifier	Exp Val
	GenPept/UniProt/Swiss-Prot A	Log Ratio
ATP5D	Q9D3D9	↓-1.553
ATP5F1	Q9CQQ7	↓-1.289
ATP5I	Q06185	↓-1.737
ATP5J2	P56135	↓-2.752
ATP5O	Q9DB20	↓-1.744
NDUFA6	Q9CQZ5	↓-2.713
NDUFB10	Q9DCS9	↓-2.455
VDAC1	Q60932	↑1.657
VDAC3	Q60931	↑1.962

OXPHOS (Oxidative Phosphorylation)

Symbol	Identifier	Exp Val
	GenPept/UniProt/Swiss-Prot A	Log Ratio
ATP5D	Q9D3D9	↓-1.553
ATP5F1	Q9CQQ7	↓-1.289
ATP5I	Q06185	↓-1.737
ATP5J2	P56135	↓-2.752
ATP5O	Q9DB20	↓-1.744
NDUFA6	Q9CQZ5	↓-2.713
NDUFB10	Q9DCS9	↓-2.455

C

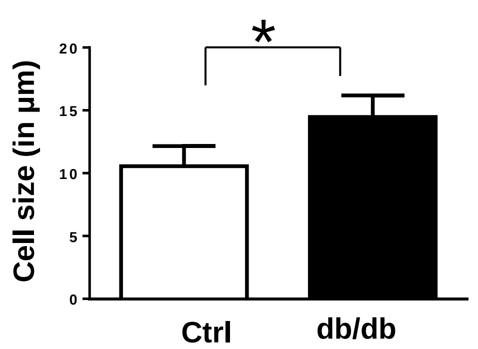

D

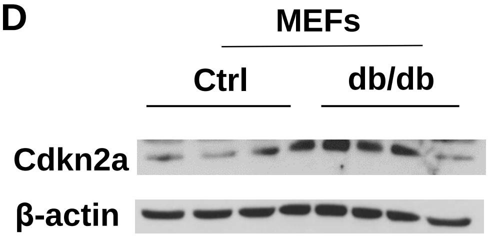

Supplemental Figure S1 : A. Heat map of differential regulated proteins between Ctrl and db/db MEFs :green represents downregulated proteins while red represents upregulated proteins in db/db MEFs; B. Differentially regulated proteins related to mitochondrial dysfunction (upper panel) and OXPHOS (lower panel); C. Quantification of Ctrl and db/db MEFs using cell counter; D. Cdkn2a protein level was upregulated in db/db MEFs. . n=3 independent experiments, data are shown as mean ± SD and student's t-test. (* $p<0.05$, ** $p<0.01$) (Related to Figure 1)

Figure S2

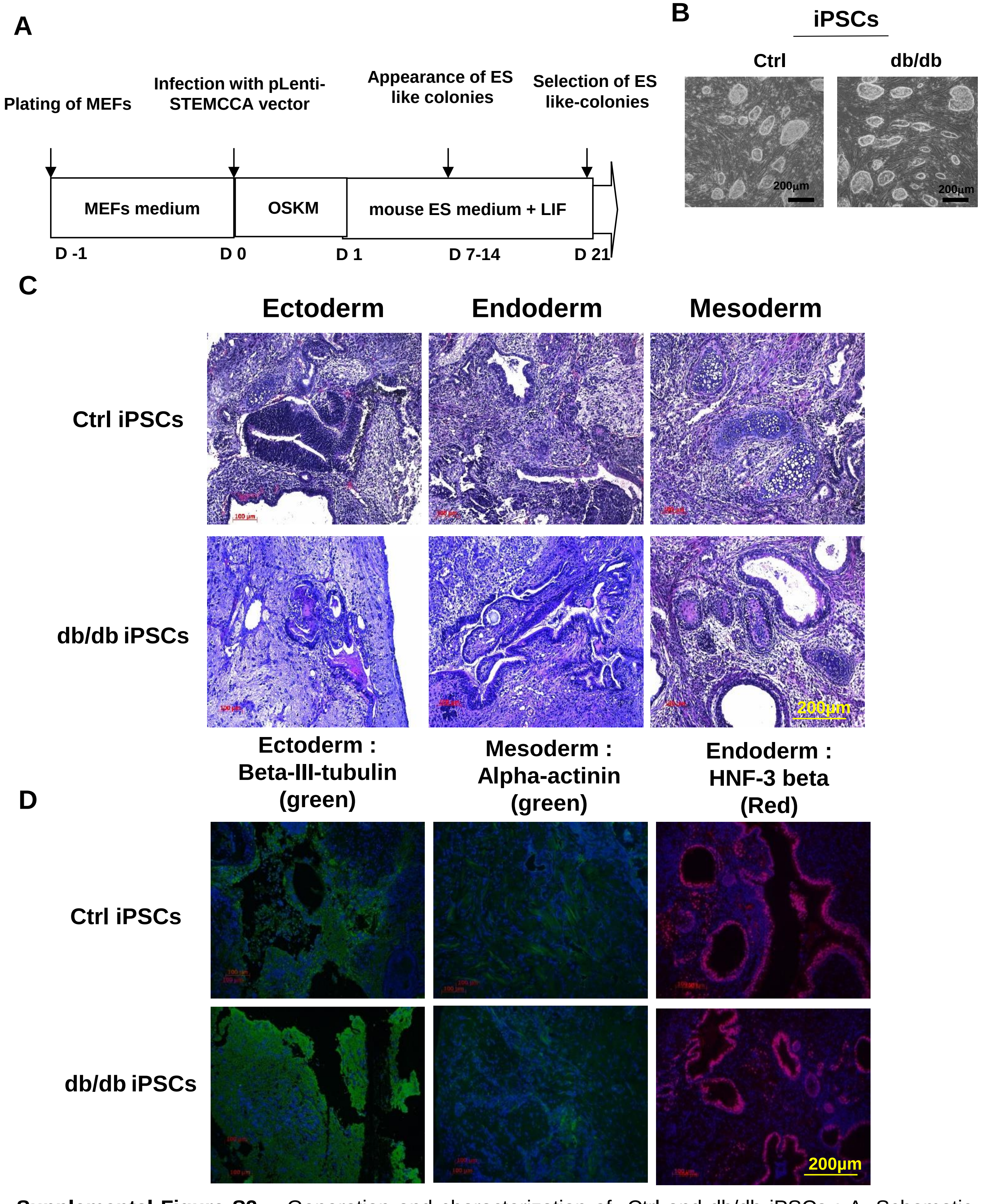

Supplemental Figure S2 : Generation and characterization of Ctrl and db/db iPSCs : A. Schematic reprogramming of mouse embryonic fibroblasts (MEFs) into induced pluripotent stem cells (iPSCs) B. Morphological images of Ctrl and db/db iPSCs , Scale bar-200µm; C. Ctrl and db/db iPSCs were injected into SCID or B6 mice and teratomas harvested after 4 weeks for analyses. H&E stainings of teratoma sections obtained from Ctrl and db/db iPSCs; D. Lineage marker staining's of teratoma sections showing the presence of the three lineage markers (Related to Figure 1) Scale bar-200µm and N=4. . n=3 independent experiments, data are shown as mean ± SD and student's t-test. (* p<0.05, ** p<0.01)

Figure S3

A

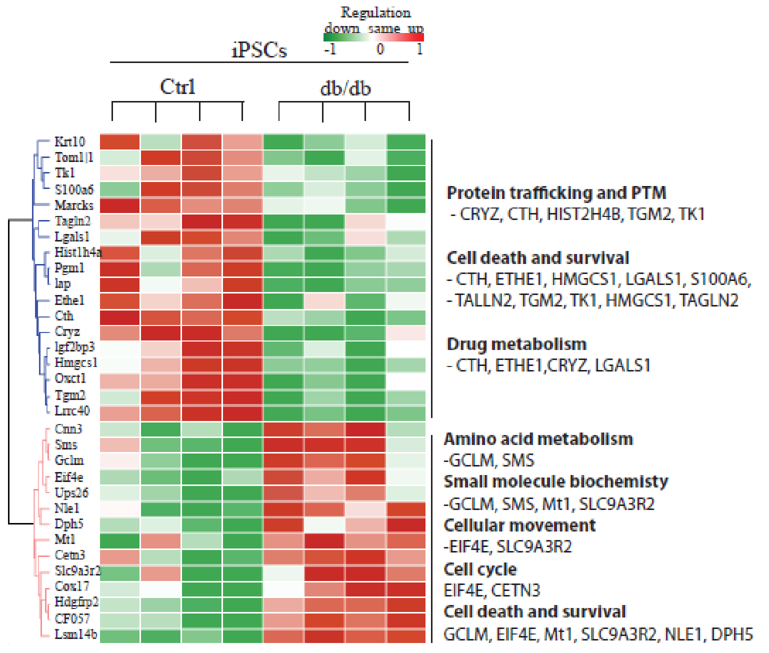

B

EIF2 signaling

Symbol	Identifier	Exp Val
	GenPept/UniProt/Swiss-Prot Ac	Log Ratio
EIF4E	P63073	↑1.287
RPL24	Q8BP67	↓-0.349
RPL28	P41105	↓-0.448
RPL10A	P53026	↓-0.266
RPL13A	P19253	↓-0.274
RPS7	P62082	↓-0.490

Oct4 signaling

Symbol	Identifier	Exp Val
	GenPept/UniProt/Swiss-Prot Ac	Log Ratio
IGF2BP1	O88477	↓-0.598
POU5F1	P20263	↓-0.581
Tdh	Q8K3F7	↓-0.581

C

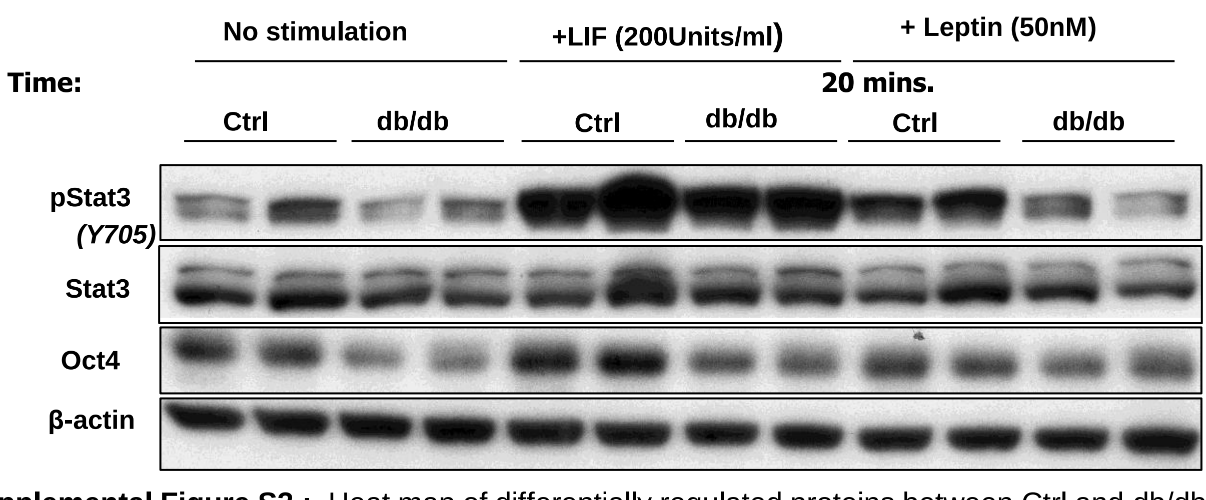

Supplemental Figure S3 : Heat map of differentially regulated proteins between Ctrl and db/db iPSCs : A. Green represents downregulated proteins while red represents upregulated proteins in db/db iPSCs; B. Differentially regulated proteins related to eukaryotic initiation factor 2 (EIF2) (protein synthesis) and octamer- binding transcription factor 4 (Oct4) (pluripotency) signaling pathways; C. Western blot analysis showing reduced phospho-Stat3 and Oct4 in db/db iPSCs. β-actin was used as a loading control. n=3 independent experiments, data are shown as mean ± SD and student's t-test. (* p<0.05, ** p<0.01) (Related to Figure 1)

Figure S4

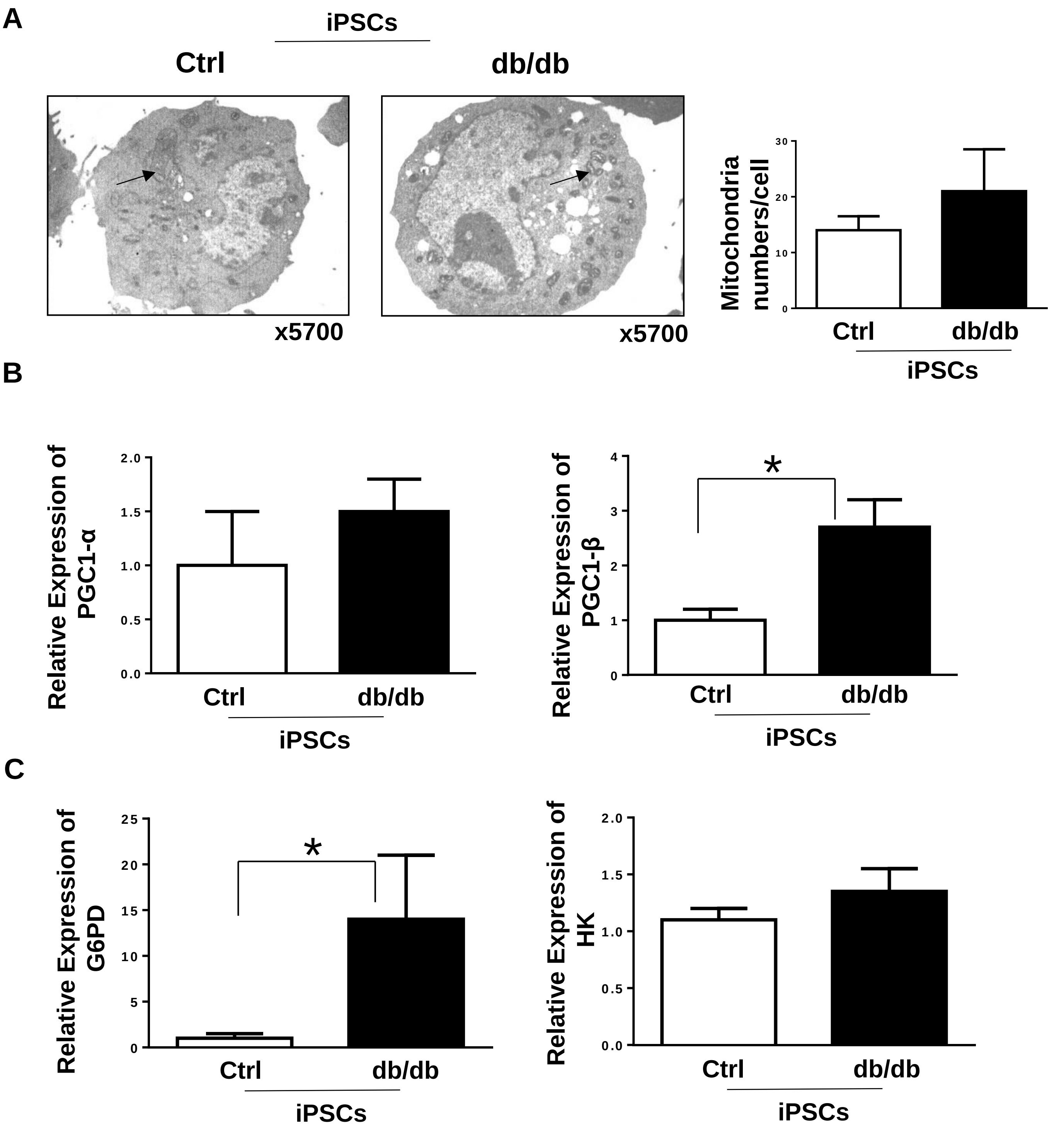

Supplemental Figure S4 : Mito OXPHOS characterization of Ctrl and db/db iPSCs: A. Electron microscopy images of iPSCs from both the groups; Black arrow indicates mitochondria inside the cell (left panel). Mitochondria quantification per cell using N=10 image each for Ctrl and db/db iPSCs (right panel) B. Real time PCR analysis of OXPHOS genes (peroxisome proliferator-activated receptor gamma Co-activator 1-alpha (PGC1-α) and peroxisome proliferator-activated receptor gamma Co-activator 1-beta PGC1-β). C Real time PCR analysis of glycolytic genes (glucose-6- phosphate dehydrogenase (G6PD) and hexokinase (HK) ,N=3 in Ctrl and db/db iPSCs. n=3 independent experiments, data are shown as mean ± SD and student's t-test. (* $p<0.05$, ** $p<0.01$) (Related to Figure 2).

Figure S5

A

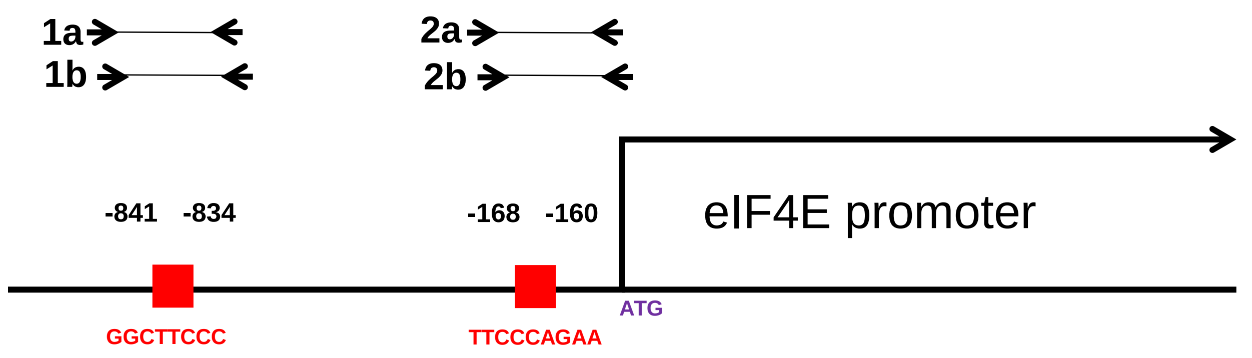

B

Dissociation curve for Stat3 primers 1a, 1b, 2a, 2b

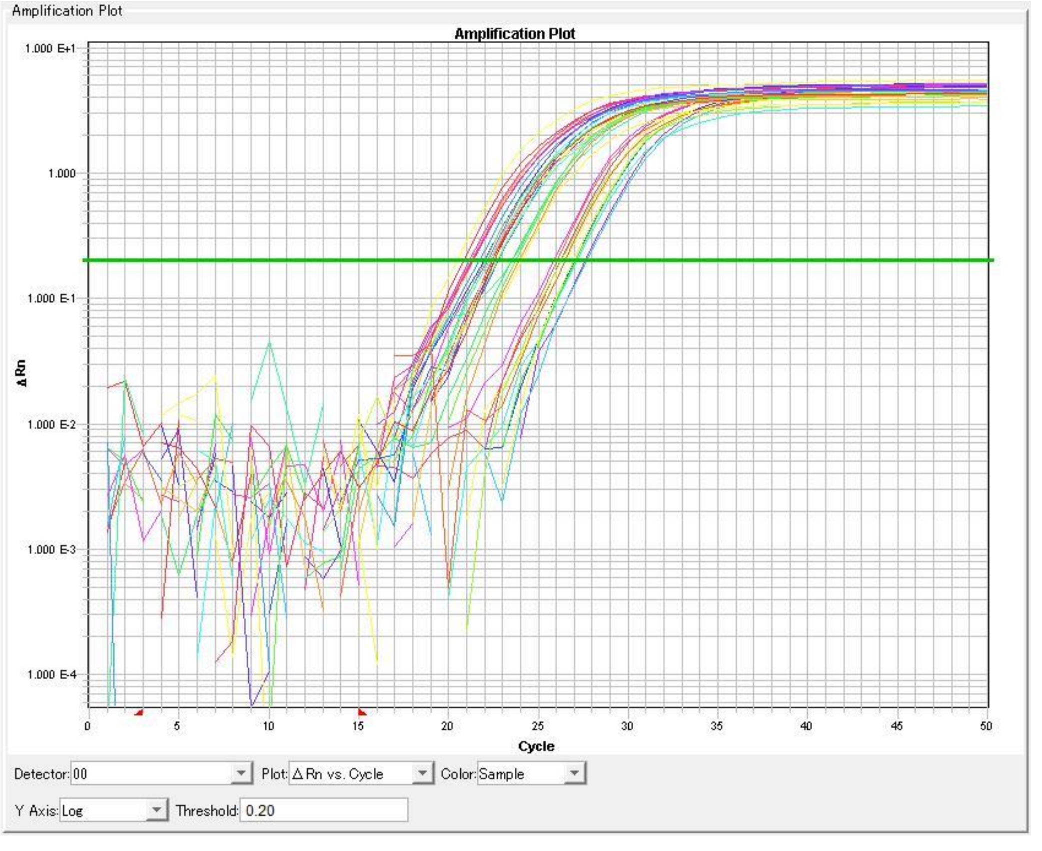

Supplemental Figure S5 : Signal transducer and activator of transcription 3 (Stat3) binding regions on the promoter of eukaryotic translation initiation actor 4E (eIF4E) : A. Two red boxes denote the Stat3 binding regions on the promoter of eIF4E ; B. Primers 1a ,1b were designed to amplify Stat3 binding region 1st while 2a, 2b were designed to amplify Stat3 binding region 2nd (Related to Figure 3 and 5)

Figure S6

A

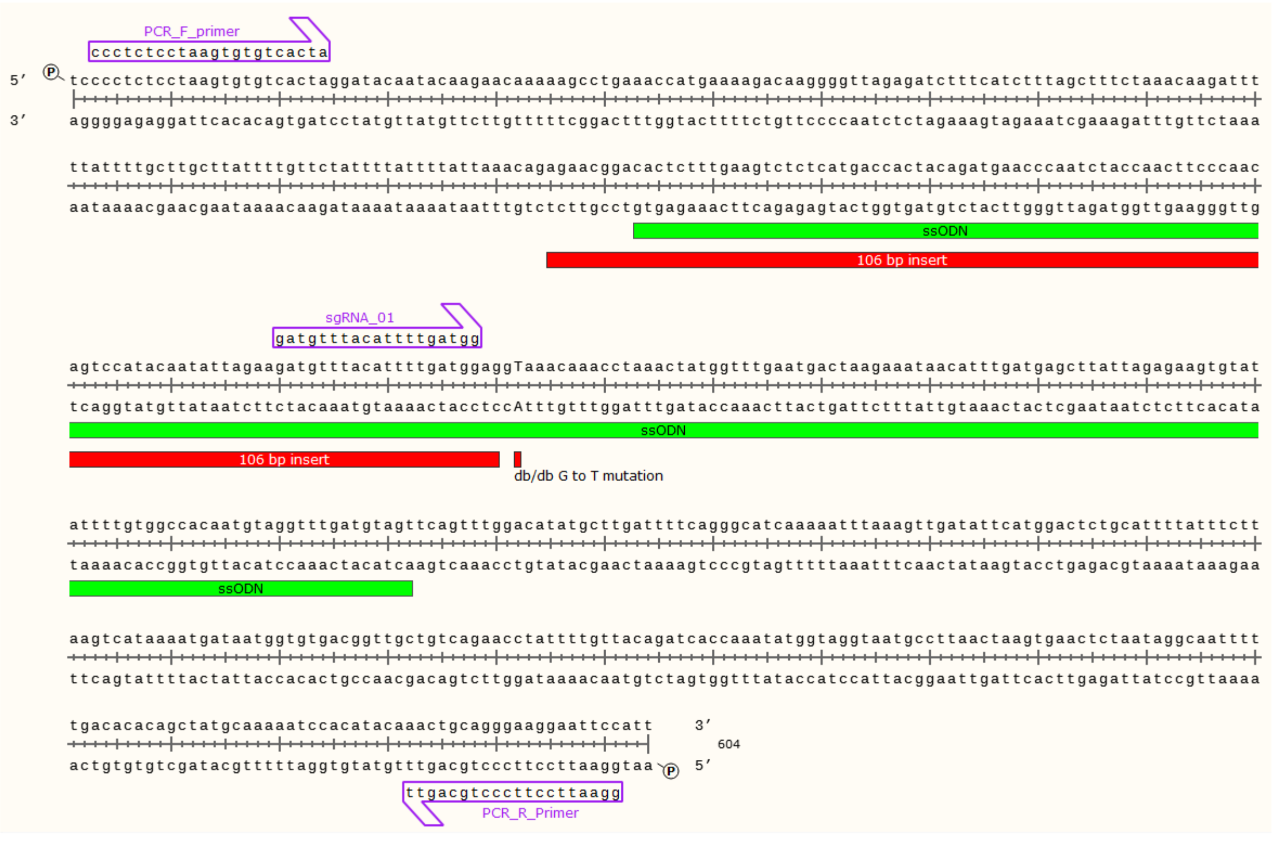

B

C

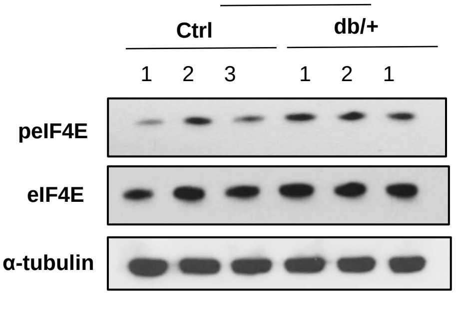

Supplemental Figure S6 : Designing the strategy for correction of db/db mutation: A. Guide RNAs specificto db/db mutation are designed along with Ctrl donor template. B. Many homozygous deletions (In dels) were found in CRISPR corrected db/db clones. C. Western blot analysis showing restoration of protein expression of peIF4E and total eIF4E in CRISPR-corrected db/db iPSCs. α-tubulin was used as a loading control. n=3 independent experiments, data are shown as mean ± SD and student's t-test. (* p<0.05, ** p<0.01). (Related to Figure 3)

Gupta et al, Supplemental materials

Experimental Procedures:

Lentiviral-mediated reprogramming and iPS cell generation and characterization

Briefly, MEFs (5 x 10^4) were plated in six well plates, and virally transduced with the lentiviral particles in the presence of 5 μg/ml Polybrene® (EMD Millipore) after 8-24 hours. The fibroblasts were washed three times with PBS and fed fresh 15% mouse embryonic stem (ES) cell media supplemented with leukemia inhibitory factor (LIF) (EMD millipore). On day 7-14, embryonic stem cell (ESC) like colonies were individually picked, cultured, expanded, frozen and subsequently characterized for pluripotency markers.

Gene expression analyses using quantitative RT-PCR and western immunoblotting

Expression of transcripts of interest was quantitated by SYBR Green-based reverse transcriptase-PCR (RT-PCR) using 2.0 µl of diluted cDNA and 8µl of SYBR Green Master Mix (Life Technologies) in a 10µl total reaction volume including primers at a concentration of 500nM each. Each PCR had three technical replicates per sample that were quantified using an ABI7600HT Sequence Detection System (Life Technologies). β-actin was used for normalization of expression of individual genes. The various antibodies were used in western blotting including OCT4 (Santa Cruz Bio.sc-5279), NANOG (Cell Signaling, 8785s), SATA3 (Santa Cruz Bio.sc-482), β-ACTIN (Santa Cruz Bio. sc-1616), pSTAT3 (Cell Signaling, 9145s), pEIF4E (Cell Signaling, 9741s), eIF4E (Cell Signaling, 9742s), pEIF4G (Cell Signaling, 2441s), EIF4G (Cell Signaling, 2469P), α-TUBULIN (Abcam, ab7291). The blots were developed using chemiluminescent substrate (low sensitivity, Pico reagent or high sensitivity, West Femto maximum sensitivity reagent) from ThermoFisher Scientific (Waltham, MA).

Immunohistochemistry

Cells were blocked by 5% donkey serum for 1 hour followed by the overnight incubation with primary antibodies chicken anti-NESTIN (1:1000, NB100-1604; Novus Biologicals), rabbit anti-NOGGIN (1:200, ab-16054, Abcam), rabbit anti-GFAP (1:1000, NB300-141, Novus Biologicals). Next day, cells were washed three times and incubated with secondary antibodies anti-chicken Alexa 488 for NESTIN, anti-rabbit Alexa 488 for GFAP, and anti-rabbit Alexa 594 for NOGGIN ; 1:1000 ,Invitrogen for 1-2 hour. DAPI was used to stain nuclei.

Teratoma sections were fixed in paraformaldehyde, processed and embedded in paraffin. All sectioning and histopathology procedures were performed at the DF/HCC Research Pathology Core. Slides were analyzed by hematoxylin and eosin staining or immunostaining with specific primary antibodies

Metabolic profiling:

Briefly, cells were cultured in non-buffered DMEM with 4.5g/l glucose. A bioenergetics profile, comprised of basal mitochondrial respiration, ATP turnover, H^+ leak, mitochondrial respiratory capacity and non-mitochondrial respiration, was determined by measuring oxygen consumption rate (OCR) in the basal state and following sequential spaced injections of oligomycin (10 μM), carbonyl cyanide p-trifluoromethoxyphenylhydrazone (FCCP) (1 μM) and rotenone (5 μM). For evaluation of glycolysis, cells were processed in non-buffered KHB buffer, followed by determination of basal respiration and the glycolytic capacity was assessed by measuring OCR in the basal state, followed by injection of 25 mM glucose and injection of 25 mM 2-deoxyglucose.

Mass spectrometry analyses

The details of the procedures used for proteomics analyses are available in Supplemental information. Briefly, cells were lysed and prepared for analysis by liquid chromatography coupled to tandem mass spectrometry (LC-MS/MS). Peptides from each cell line were labeled using isobaric tags (Tandem Mass Tags, TMT, Thermo Fischer Scientific, Bremen, Germany) and multiplexed in equal amounts, experimental design in Supplemental information. Each multiplexed sample was subjected to fractionation prior to LC-MS/MS analysis on an LTQ Orbitrap Elite coupled to a Dionex Ultimate NCS-3000 LC system (both Thermo Fischer Scientific, Bremen, Germany).

Details regarding the mass spectrometry data interpretation are available in Supplemental information. Briefly, raw mass spectrometry data were converted using MSConvert as part of the ProteoWizard (Chambers et al. 2012) package, and searched with OMSSA (Geer et al. 2004) and X! Tandem (Craig and Beavis 2004) *via* SearchGUI (Vaudel et al. 2011). Search engine results were processed using PeptideShaker (Vaudel et al. 2015). Notably, so-called protein ambiguity groups were built based on the unicity of peptide sequences in proteins as described in (Nesvizhskii and Aebersold 2005). Proteins identified by mass spectrometry will implicitly refer to protein ambiguity groups. All identification results were validated at a 1% False Discovery Rate (FDR) threshold estimated using the target/decoy strategy (Elias and Gygi 2010). Proteins abundances were inferred from the reporter ion intensities using Reporter (http://compomics.github.io/projects/reporter.html).

Supplemental methods for the Proteomic analyses

Chemicals

Bicinchoninic acid assay (BCA) protein assay kit was purchased from Novagen® (EMD Chemicals, San Diego, CA, USA). TMT sixplex™ Isobaric Mass Tagging Kit, including Pierce™ Trypsin Protease (MS grade), were purchased from Thermo Scientific (Rockford, IL, USA). Water, acetonitrile (ACN), and formic acid (FA), all MS-grade, were purchased from Sigma-Aldrich (St. Louis, MO, USA).

Cell lysis and protein digestion

Cells were lyzed using M-Per mammalian protein extraction buffer and protein concentration was determined using a BCA protein assay kit. Dry aliquots containing an estimated amount of 50 µg of proteins were reduced, alkylated and digested overnight according to the Tandem Mass Tagging (TMT) kit vendor's instructions. Briefly, samples were re-suspended in 8 M urea, followed by addition of 100 mM Triethyl Ammonium Bicarbonate (TEAB). The volume was adjusted with milliQ water to reach a final protein concentration of 5 µg/µL. Protein disulfide bonds were reduced by the addition of 200 mM Tris(2-carboxyethyl)phosphine hydrochloride (TCEP) and incubated for one hour at room temperature (RT). Free sulfhydryl groups were subsequently alkylated by the addition of 375 mM Iodoacetamide (IAA) dissolved in 100 mM TEAB, for 30 min in the dark at RT. The protein mixture was diluted 6 times with pre-chilled acetone (-20 °C) to allow for precipitation for 16 h at -20 °C. After centrifugation at 8,000 x g for 10 min at 4 °C, the acetone was gently removed and the sample dried. Proteins were re-suspended in 50 µL 100 mM TEAB and digested overnight (37 °C) using trypsin, at a protease to protein ratio of 1:40.

Tandem Mass Tag (TMT) 6-plex Labeling

Tryptic digests were labeled with Tandem Mass Tag TMT 6-plex reagents according to the manufacturer's protocol, and combined. Three TMT 6-plex labeling sets were used for the twelve samples included in this study, samples were randomly assigned to four labels TMT^6-128-131. Two common reference samples containing equal amounts from each individual sample were labeled TMT^6-126 and TMT^6-127. Sample repartition is detailed in Table 1.

Sample Fractionation

Labeled peptide samples were pre-fractionated by mixed mode reversed phase-anion exchange (MM RP-AX) as described in (Phillips et al. 2010), using a Promix MP 250 mm x 2.1 mm id, pore size 300Å column (SIELC Technologies, Prospect Hights, IL, USA) connected to an Agilent Technology 1260 off-line LC-system. Each of the three combined samples (Set 1, 2, 3) was re-suspended in 120 μL solvent A (20mM ammonium formate/ 3% acetonitrile (ACN), pH 6.5) and loaded onto the column. Column flow was set to 50 μL/min and gradient length was 70 min. From 0-45 min solvent B (2mM ammonium formate/ 80% ACN) increased linearly from 15% to 60%, from 45-55 min 60% B, from 55-65 min 100% B and from 65-70 min 15% B. The samples were separated during equal time intervals into 60 fractions. (The eight first fractions containing TMT-reagent debris were discarded. Fractions at each end of the gradient were combined to give the total number of representative fractions of 39. Fractions 9-11 and 12-14 were combined, as well as fractions 49-51, 52-54, and 55-60).

LC-MS/MS analysis

In total, 117 fractions were obtained from the twelve initial protein lysates (39 fractions x 3). From each of these, 0.5 μg was dissolved in 1% aqueous formic acid (FA) prior to LC-MS/MS analysis on an LTQ-Orbitrap Elite mass spectrometer, equipped with a nanospray Flex ion source, and coupled to a Dionex Ultimate NCS-3000 LC system (all from Thermo Fischer Scientific, Bremen, Germany).

The samples were loaded and desalted on a pre-column (Acclaim PepMap 100, 2 cm x 75 μm i.d. nanoViper column, packed with 2 μm C18 beads) at a flow rate of 5 μL/min for 6 min using an isocratic flow of 0.1% FA and 2% ACN. Peptides were separated during a biphasic ACN gradient from two nanoflow UPLC pumps with a flow rate of 280 nL/min on the analytical column (Acclaim PepMap 100, 15 cm x 75μm i.d. nanoViper column, packed with 2μm C18 beads). Solvent A was 0.1% FA and 2% ACN. Solvent B was 0.1% FA and 90 % ACN. The gradient was 0-61.5 min ramp from 8–38% B, 61.5-64.5 min ramp from 38–90% B, 64.5-69.5 min 90% B followed by column conditioning for 12 minutes with 5% B.

The ten most intense ions in every survey scan were subjected to higher energy collision dissociation (HCD) with a normalized collision energy of 40%, a default charge state of 2 and an activation time of 0.100 ms, accounting for a dynamic exclusion of 25 s. Survey full scan MS spectra (from *m/z* 300-2000) were acquired at a resolution of 60,000 at *m/z* 400. MS data were acquired over 90 minutes.

Data interpretation

The acquired raw data files were converted to peak lists using MSConvert as part of the ProteoWizard (Kessner et al. 2008) package, and searched using OMSSA (Geer et al. 2004) version 2.1.9 and X!Tandem (Craig and Beavis 2004) version Sledgehammer (2013.09.01.1) *via*

SearchGUI (Vaudel et al. 2011) version 1.16.0 against a concatenated target/decoy version of the *Mouse musculus* reviewed complement of the UniProtKB (Apweiler et al. 2004) database (downloaded November 2013, 16, 656 target sequences) where decoy sequences are the reversed version of the target as generated by SearchGUI. The search settings were: carbamidomethylation of Cys (+57.021464 Da), TMT 6-plex on peptide N-term peptide and Lys (+229.162932 Da) as fixed modifications; oxidation of Met (+15.994915 Da) as variable modification; precursor mass tolerance 10.0 ppm; fragment mass tolerance 0.5 Da; trypsin as enzyme allowing maximum of two missed cleavages. All other settings were set to the defaults of SearchGUI.

Search engine results were processed using PeptideShaker version 0.25.0 (Vaudel et al. 2015) Briefly, peptide spectrum matches (PSMs) were assembled into peptides and proteins and the identification results were validated at a 1% False Discovery Rate (FDR) threshold estimated using the target and decoy distributions of matches (Elias and Gygi 2010), a confidence level is provided for every match as complement of the Posterior Error Probability (PEP) estimated using the target and decoy distributions of matches (Nesvizhskii 2010). Protein ambiguity groups were built based on the unicity of peptide sequences in proteins as described in (Nesvizhskii and Aebersold 2005), and a representative protein was chosen for every group based on the evidence level provided by UniProt. In the following, proteins identified by mass spectrometry will implicitly refer to protein ambiguity groups.

Proteins were quantified using Reporter version of November 2013 (http://compomics.github.io/projects/reporter.html). Briefly, for every validated protein, the TMT reporter ions were extracted from spectra of validated PSMs and deisotoped using the isotope abundance matrix (Vaudel et al. 2010) provided by the manufacturer. Intensities were normalized using the median intensity in order to limit the ratio deviation (Vaudel et al. 2014) and peptide and protein ratios were estimated using maximum likelihood estimators (Burkhart et al. 2011). The median of the reference channels was used as reference and sample to reference ratios were estimated for all samples. Ratios were $\log_2$ converted and normalized to the median to avoid inter-sample bias. Only those proteins presenting two or more validated and quantitated peptides were retained for further analysis. Standard contaminants were excluded from downstream statistical analysis.

Unsupervised hierarchical clustering

Unsupervised hierarchical were performed in Perseus (v.1.6.2.3) on z-normalized abundance values. The parameters for clustering were average linkage and euclidean correlation as distance measurement, prepossessed with k-means.

Statistical analysis

The significance of the protein regulation between different cell types was evaluated using a student's t-test and a p-value <0.05 was considered significant. Volcano plots were created by plotting the p-value against the regulation level. Significantly regulated proteins were separated into three groups according to the measured regulation level: (1) background (ratio between 0.5:1 and 2:1); (2) moderately regulated (ratio between 0.1:1 and 0.5:1 or 2:1 and 10:1); and strongly regulated (ratio lower than 0.1:1 or higher than 10:1). Hierarchical clustering was conducted using Perseus as part of the MaxQuant software suite (Cox and Mann 2008).

Supplemental methods for the RNAseq analyses

Data

RNA-seq raw reads are downloaded from DNA Link, which are reversely-stranded paired-end reads. The counts table tx2gene_counts_mmu.rds is generated by aligning reads to the mouse transcriptome (Ensembl version 94) using kallisto (Bray et al. 2016) and converting transcript counts to gene counts using tximport (Soneson et al. 2015).

The phenotype information is in table pheno_mouse.csv.

Filtering, normalization, and transformation

To filter out low expressing genes, we keep genes that have counts per million (CPM) more than 1 in at least 4 samples. There are 14245 genes after filtering. We then normalize counts by weighted trimmed mean of M-values (TMM) (Robinson and Oshlack 2010). The normalization factors are between 0.93 and 1.08.

In order to use linear models in the following analysis, we perform Voom transformation (Law et al. 2014) to transform counts into logCPM, where CPM = 1e+6 * count of a gene / (total counts of the sample * normalization factor of the sample). Voom transformation also estimates the mean-variance relationship and use it to compute appropriate observation-level weights, so that more read depth gives more weights.

PCA

To get an overall view of the similarity and/or difference of the samples, we perform principal component analysis (PCA). The PCA plot pca.pdf shows that samples are clustered by groups and there is an outlier aB6_A5_2 (shown in the labeled PCA plot pca_labeled.pdf). Therefore we remove the outlier and redo the PCA pca_no_outlier.pdf.

Linear modeling

To discover the differential genes, we use limma, an R package that powers differential expression analyses (Ritchie et al. 2015). We account for the correlation of technical replicates in the analysis. We perform moderated t-test to detect genes that are differentially expressed between mutants and controls.

In the p-value distribution pval_dist.pdf, the Q-Q plot shows that we observe more significant p-values than expect, and the histogram shows that there is substantial enrichment of significant p-values and the proportion of the true null hypothesis is less than 50%.

Gene statistics table for all genes gene_stats.csv. The table contains the average logCPM of each group, p-values, FDR, log fold-change, fold-change, and gene annotation. Genes with FDR < 0.25 are considered significantly changed.

Plots

In the volcano plots volcanoes.pdf, the top genes of either smallest p-values or largest logFC are labeled.

In the dot plots top_genes_dotplots.pdf, top genes (according to p-values) are selected and the logCPM are plotted.

In the heatmap top_genes_heat.pdf, the same set of top genes are used as in dot plots. The z-scores of the logCPM are plotted.

Pathway analysis

We obtain the Gene sets from the MSigDB Collections. We select the gene sets that belong to the canonical pathways (CP), gene motif (transcription factor targets or microRNA targets), and gene ontology (GO).

We then use the Fry function of the Rotation Gene Set Test (Roast) in the limma R package to perform pathway analysis (Wu et al. 2010). This will tell us if all the genes in a pathway gene set are directionally or undirectionally (i.e. mixed) changed. The results are in tables cp_fry.xlsx; motif_fry.xlsx; go_fry.xlsx.

We also use the Fisher Exact test to determine if the gene lists in Gene list for heat maps in db project.csv are over presneted in pathway gene sets.

Supplemental References:

Apweiler R, Bairoch A, Wu CH, Barker WC, Boeckmann B, Ferro S, Gasteiger E, Huang H, Lopez R, Magrane M et al. 2004. UniProt: the Universal Protein knowledgebase. *Nucleic Acids Res* **32**: D115-119.

Bray NL, Pimentel H, Melsted P, Pachter L. 2016. Near-optimal probabilistic RNA-seq quantification. *Nature biotechnology* **34**: 525-527.

Burkhart JM, Vaudel M, Zahedi RP, Martens L, Sickmann A. 2011. iTRAQ protein quantification: a quality-controlled workflow. *Proteomics* **11**: 1125-1134.

Chambers MC, Maclean B, Burke R, Amodei D, Ruderman DL, Neumann S, Gatto L, Fischer B, Pratt B, Egertson J et al. 2012. A cross-platform toolkit for mass spectrometry and proteomics. *Nature biotechnology* **30**: 918-920.

Cox J, Mann M. 2008. MaxQuant enables high peptide identification rates, individualized p.p.b.-range mass accuracies and proteome-wide protein quantification. *Nature biotechnology* **26**: 1367-1372.

Craig R, Beavis RC. 2004. TANDEM: matching proteins with tandem mass spectra. *Bioinformatics* **20**: 1466-1467.

Elias JE, Gygi SP. 2010. Target-decoy search strategy for mass spectrometry-based proteomics. *Methods Mol Biol* **604**: 55-71.

Geer LY, Markey SP, Kowalak JA, Wagner L, Xu M, Maynard DM, Yang X, Shi W, Bryant SH. 2004. Open mass spectrometry search algorithm. *J Proteome Res* **3**: 958-964.

Kessner D, Chambers M, Burke R, Agus D, Mallick P. 2008. ProteoWizard: open source software for rapid proteomics tools development. *Bioinformatics* **24**: 2534-2536.

Law CW, Chen Y, Shi W, Smyth GK. 2014. voom: Precision weights unlock linear model analysis tools for RNA-seq read counts. *Genome Biol* **15**: R29.

Nesvizhskii AI. 2010. A survey of computational methods and error rate estimation procedures for peptide and protein identification in shotgun proteomics. *Journal of proteomics* **73**: 2092-2123.

Nesvizhskii AI, Aebersold R. 2005. Interpretation of shotgun proteomic data: the protein inference problem. *Molecular & cellular proteomics : MCP* **4**: 1419-1440.

Phillips HL, Williamson JC, van Elburg KA, Snijders AP, Wright PC, Dickman MJ. 2010. Shotgun proteome analysis utilising mixed mode (reversed phase-anion exchange chromatography) in conjunction with reversed phase liquid chromatography mass spectrometry analysis. *Proteomics* **10**: 2950-2960.

Ritchie ME, Phipson B, Wu D, Hu Y, Law CW, Shi W, Smyth GK. 2015. limma powers differential expression analyses for RNA-sequencing and microarray studies. *Nucleic Acids Res* **43**: e47.

Robinson MD, Oshlack A. 2010. A scaling normalization method for differential expression analysis of RNA-seq data. *Genome Biol* **11**: R25.

Soneson C, Love MI, Robinson MD. 2015. Differential analyses for RNA-seq: transcript-level estimates improve gene-level inferences. *F1000Res* **4**: 1521.

Vaudel M, Barsnes H, Berven FS, Sickmann A, Martens L. 2011. SearchGUI: An open-source graphical user interface for simultaneous OMSSA and X!Tandem searches. *Proteomics* **11**: 996-999.

Vaudel M, Burkhart JM, Zahedi RP, Oveland E, Berven FS, Sickmann A, Martens L, Barsnes H. 2015. PeptideShaker enables reanalysis of MS-derived proteomics data sets. *Nature biotechnology* **33**: 22-24.

Vaudel M, Sickmann A, Martens L. 2010. Peptide and protein quantification: a map of the minefield. *Proteomics* **10**: 650-670.

-. 2014. Introduction to opportunities and pitfalls in functional mass spectrometry based proteomics. *Biochimica et biophysica acta* **1844**: 12-20.

Wu D, Lim E, Vaillant F, Asselin-Labat ML, Visvader JE, Smyth GK. 2010. ROAST: rotation gene set tests for complex microarray experiments. *Bioinformatics* **26**: 2176-2182.